Low-Loss Si_3N_4 TriPleX Optical Waveguides: Technology and Applications Overview

Chris G. H. Roeloffzen, Marcel Hoekman, Edwin J. Klein, Lennart S. Wevers, Roelof Bernardus Timens, Denys Marchenko, Dimitri Geskus, Ronald Dekker, Andrea Alippi, Robert Grootjans, Albert van Rees, Ruud M. Oldenbeuving, Jörn P. Epping, René G. Heideman, Kerstin Wörhoff, Arne Leinse, Douwe Geuzebroek, Erik Schreuder, Paulus W. L. van Dijk, Ilka Visscher, Caterina Taddei, *Member, IEEE*, Youwen Fan, Caterina Taballione, Yang Liu, David Marpaung, Leimeng Zhuang, Meryem Benelajla, and Klaus-J. Boller

(Invited Paper)

***Abstract*—An overview of the most recent developments and improvements to the low-loss TriPleX Si_3N_4 waveguide technology is presented in this paper. The TriPleX platform provides a suite of waveguide geometries (box, double stripe, symmetric single stripe, and asymmetric double stripe) that can be combined to design complex functional circuits, but more important are manufactured in a single *monolithic* process flow to create a compact photonic integrated circuit. All functionalities of the integrated circuit are constructed using standard basic building blocks, namely straight and bent waveguides, splitters/combiners and couplers, spot size converters, and phase tuning elements. The basic functionalities that have been realized are: ring resonators and Mach–Zehnder interferometer filters, tunable delay elements, and waveguide switches. Combination of these basic functionalities evolves into more complex functions such as higher order filters, beamforming networks, and fully programmable architectures. Introduction of the *active* InP chip platform in a combination with the TriPleX will introduce light generation, modulation, and detection to the low-loss platform. This *hybrid* integration strategy enables fabrication of tunable lasers, fully integrated filters, and optical beamforming networks.**

***Index Terms*—Beam steering, integrated optics, lasers, optical communication, optical filters, optical waveguides.**

Manuscript received September 29, 2017; revised January 10, 2018; accepted January 10, 2018. Date of publication January 15, 2018; date of current version February 14, 2018. *(Corresponding author: Chris G. H. Roeloffzen.)*

C. G. H. Roeloffzen, M. Hoekman, E. J. Klein, L. S. Wevers, R. B. Timens, D. Marchenko, D. Geskus, R. Dekker, A. Alippi, R. Grootjans, A. van Rees, R. M. Oldenbeuving, J. P. Epping, R. G. Heideman, K. Wörhoff, A. Leinse, D. Geuzebroek, E. Schreuder, P. W. L. van Dijk, and I. Visscher are with the LioniX International BV, Enschede AL 7500, The Netherlands (e-mail: c.g.h.roeloffzen@lionix-int.com; m.Hoekman@Lionix-int.com; e.j.klein@lionix-int.com; l.Wevers@Lionix-int.com; r.b.timens@lionix-int.com; d.Marchenko@Lionix-int.com; d.Geskus@Lionix-int.com; r.Dekker@Lionix-int.com; A.Alippi@lionix-int.com; r.grootjans@lionix-int.com; albertvanrees@gmail.com; r.m.oldenbeuving@lionix-int.com; j.p.Epping@Lionix-int.com; r.g.Heideman@Lionix-int.com; k.Worhoff@Lionix-int.com; a.leinse@lionix-int.com; d.h.geuzebroek@lionix-int.com; f.Schreuder@Lionix-int.com; p.w.l.vandijk@lionix-int.com; i.visscher@lionix-int.com).

C. Taddei and Y. Fan are with the LioniX International BV, Enschede AL 7500, The Netherlands, and also with the University of Twente, Laser Physics and Nonlinear Optics Group, MESA+Research Institute for Nanotechnology, Enschede AE 7500, The Netherlands (e-mail: C.Taddei@lionix-int.com; y.fan@utwente.nl).

C. Taballione, M. Benelajla, and K.-J. Boller are with the University of Twente, Laser Physics and Nonlinear Optics Group, MESA+Research Institute for Nanotechnology, Enschede AE 7500, The Netherlands (e-mail: c.taballione@utwente.nl; meriembenelajla@gmail.com; k.j.boller@utwente.nl).

Y. Liu and D. Marpaung are with the Centre for Ultrahigh Bandwidth Devices for Optical Systems, University of Sydney, NSW 2006, Australia (e-mail: yliu3472@uni.sydney.edu.au; david.marpaung@sydney.edu.au).

L. Zhuang is with the Electro-Photonics Laboratory, Electrical and Computer Systems Engineering, Monash University, Clayton, VIC 3800, Australia (e-mail: leimeng.zhuang@monash.edu).

Color versions of one or more of the figures in this paper are available online at http://ieeexplore.ieee.org.

Digital Object Identifier 10.1109/JSTQE.2018.2793945

I. Introduction

SILICON photonics has reached significant interest in the last 15 years [1] for applications in datacom and telecommunications.

The manufacturing of silicon photonics circuitry shows great similarity with manufacturing process flows of microelectronics circuits and requires lithography equipment to accurately pattern the planar silicon wires to guide the light. The transparency of silicon waveguides for wavelengths between 1100 nm and 1550 nm is compatible with the use of optical fibers for optical signal transport. Silicon nitride, especially high-quality Si_3N_4, extends the usable spectral window towards 405 nm [2]. The high index contrast of silicon nitride with respect to silicon oxide makes it a perfect candidate for production of compact photonic circuitry for both infrared and visible light applications. This paper reports on numerous different applications of different types of silicon nitride waveguides, each with its specific and unique optical confinement and transmission properties.

With the development of several different, standardized, building blocks that can be *monolithically* combined in the manufacturing process flow, complex functions can be obtained that can serve application domains such as high-speed and high-capacity optical communication, microwave photonics and medical diagnostics, to mention a few.

Moreover, the development of several tool kits, product development tool kits (PDKs), for circuitry design, mask layout and performance simulation of these photonic devices, has improved the access to this field of integrated photonics. The user-friendliness and availability of the right tools supports the foundries that provide access to manufacturing line in the form

of multi-project wafer (MPW) service, where industrial and academic customers share the cost in a rapid prototyping shuttle run.

A big challenge for both silicon photonics and silicon nitride waveguides, is the integration of *active* sources such as lasers and amplifiers. Although a breakthrough was reported by Intel in 2005 [3], where they presented their continuous silicon laser, alternatives to interface and integrate lasers with the *passive* silicon platform are still investigated. This paper presents a novel approach of a planar integration strategy of InP and Si_3N_4 photonic circuits. It highlights the most important interface and assembly challenges, which have successfully been overcome, and resulted in a new world-record-performance for a narrow-linewidth hybrid laser. This hybrid approach is the foundation for the design and fabrication of more complex devices and modules that are built from *hyperfunctional* InP and Si_3N_4 chips. The requirement to develop a means and capability to fabricate these products in an economical way in medium to high volume is evident and drives the need for process optimization, automation and standardization of processes and workflows.

The structure of the paper is organized as follows. Chapter II describes the properties of silicon nitride (Si_3N_4) waveguide structures, particularly TriPleX geometries and their fabrication processes. The descriptions of *basic building blocks*, straight and bent waveguides, splitters/combiners and couplers, spot size converters and phase tuning elements, are given in Chapter III. Chapter IV describes *basic functionalities*, such as ring resonator, Mach-Zehnder interferometer filters, delays and switches. These functionalities are combinations of the basic building blocks. More complex functionalities, with higher level of integration, are described in Chapter V. Combination of *passive* and *active* functions, using hybrid integration of InP and TriPleX, is described in Chapter VI. The paper ends with Chapter VII giving a prospect of these technologies for future applications.

II. TriPleX Waveguides; Modeling

TriPleX waveguides are a family of waveguide geometries that is based on an alternating layer stack consisting of two materials: Si_3N_4 (silicon nitride) and SiO_2 (silicon dioxide) that have refractive indices of about 1.98 and 1.45, *resp.*, at 1.55 μm wavelength. Most commonly used substrate is single-crystal silicon, for some applications fused silica glass substrates have been used too (e.g., if a transparent chip in the visible light region is required). Table I demonstrates cross-sections and SEM photographs of four different waveguide geometries that will be described in more details in Sections II-A to II-D. An overview of the manufacturing process can be found in Section II-E.

A. Box Shell

The box shell geometry consists of a SiO_2 box-shaped core surrounded by a Si_3N_4 shell. Two geometries have been defined: a low-index-contrast (LIC) variant, which allows for low-loss coupling of light to or from a glass fiber, and a high-index-contrast (HIC) variant, which allows for compact device layouts because of a small bending radius. The LIC geometry optimized for telecom applications at 1.55 μm wavelength consists of a 1×1 μm^2 SiO_2 core surrounded by a 50 nm thick Si_3N_4 shell [5], while the HIC geometry has a 0.5×0.5 μm^2 core surrounded by a 170 nm shell [6]. A noteworthy property of the box shell geometry is that optical birefringence caused by material anisotropy can be compensated for by geometrical anisotropy [7]. The bending radius and mode-field diameters (MFDs) are: $R = 500$ μm, $\mathrm{MFD_{x\times y}} = 3.6 \times 3.6$ μm for the LIC geometry and $R = 150$ μm, $\mathrm{MFD_{x\times y}} = 1.4 \times 1.4$ μm for the HIC geometry. If a mode-field diameter is specified in this article, it refers to the diameter where the optical power has dropped to $1/e^2$ of the maximum intensity.

TABLE I
Schematic Layout of TriPleX Geometries and SEM Images of Realized Structures That Allow for Low Optical Propagation Loss: Box Shell (A), Single-Stripe (B), Symmetric Double-Stripe (C), and Asymmetric Double-Stripe (D) [4]

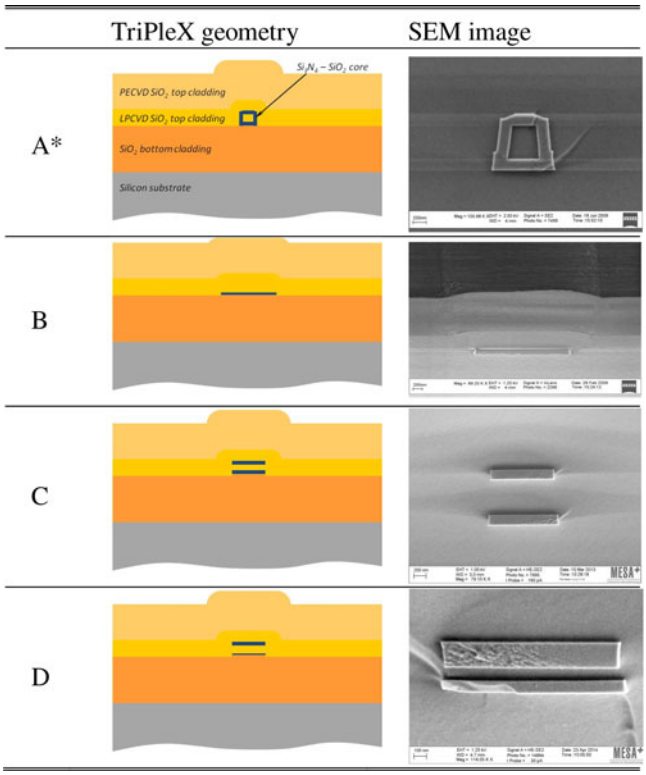

Depending on the layer thicknesses LIC and HIC versions of A-to-D exist.
*The deposition techniques are discussed in Section II-E.

B. Single-Stripe

The single-stripe geometry consists of a single Si_3N_4 stripe and is the most interesting geometry for achieving ultra-low-loss propagation on-chip. This can be realized by choosing the stripe thickness in the range of several tens of nm, and by optimizing the stripe width [8]. However, the low propagation loss is at the cost of a large bending radius in the order of thousands of μm. Propagation losses as low as 0.03 dB/cm have been achieved at 1.55 μm wavelength, using a bending radius of $R = 2000$ μm, see also Section V-D. A further reduction of these propagation losses has been achieved by replacing the PECVD SiO_2 layer in the top cladding by a bonded thermally grown SiO_2 film [9]. A single-mode single-stripe of 50 nm thickness and 5.3 μm width

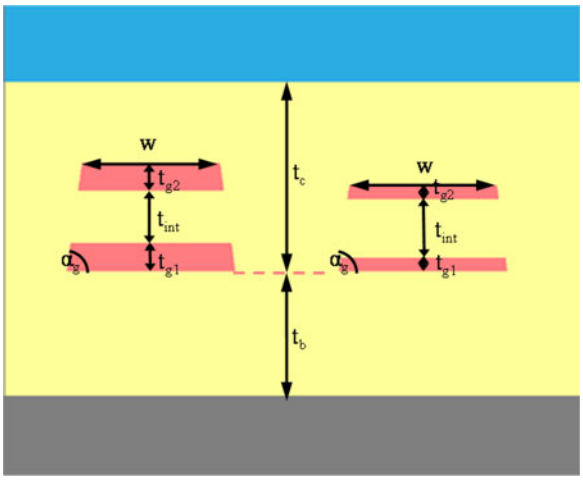

Fig. 1. Schematic cross-section of the standard TriPleX SDS waveguide for the TE_{00} mode at 1.55 μm wavelength: on the left-hand side is the HIC waveguide with stripe thicknesses $t_{g1} = t_{g2} = 170$ nm; on the right-hand side is the LIC waveguide with stripe thicknesses $t_{g1} = t_{g2} = 35$ nm; same for both HIC and LIC: intermediate layer thickness $t_{int} = 0.5$ μm, a waveguide width of $w = 1.2$ μm, and an etching angle of $\alpha_g = 82°$. Typical layer thicknesses for the SiO_2 bottom cladding t_b and for the SiO_2 top cladding t_c are 8 or 15 μm. Color legend: $= Si_3N_4$, $= SiO_2$, $=$ Si substrate, $=$ background material (e.g., air).

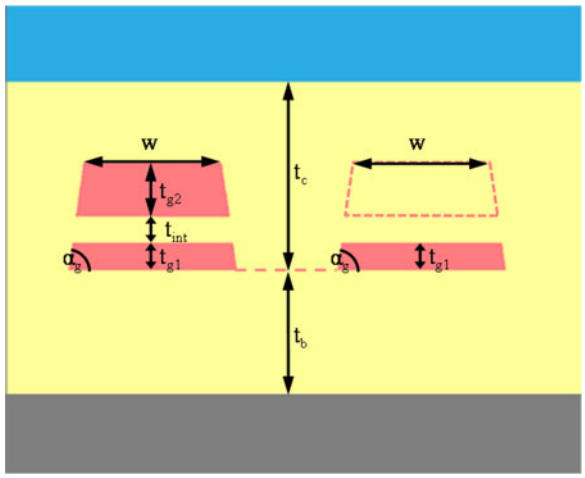

Fig. 2. Schematic cross-section of the standard TriPleX ADS waveguide for the TE_{00} mode at 1.55 μm wavelength: on the left-hand side is the HIC waveguide, with bottom stripe thickness $t_{g1} = 75$ nm, intermediate layer thickness $t_{int} = 100$ nm, top stripe thickness $t_{g2} = 175$ nm, a waveguide width of $w = 1.1$ μm, and an etching angle of $\alpha_g = 82°$; on the right-hand side is the LIC waveguide, made by locally removing the top Si_3N_4 layer after deposition of the ADS layer stack. Typical layer thicknesses for the SiO_2 bottom cladding t_b and for the SiO_2 top cladding t_c are 8 or 15 μm. Color legend: $= Si_3N_4$, $= SiO_2$, $=$ Si substrate, $=$ background material (e.g., air).

processed in this way has shown a loss of 0.007 dB/cm [10], while the best result of 0.001 dB/cm obtained so far was on single-stripe geometries at 1.58 μm wavelength: one of 40 nm thickness and 13 μm width, and another of 50 nm thickness and 6.5 μm width [9].

C. Symmetric Double-Stripe or SDS

The symmetric double-stripe (SDS) geometry consists of two stripes of Si_3N_4 of the same thickness at the top on top of each other, separated by an intermediate SiO_2 layer. The optimized geometry that is also offered in the current TriPleX IR MPW runs and has been used in many optical beam-forming networks (OBFN) devices [11], that is discussed more elaborately in Section VI-C. A schematic cross-section of the HIC SDS can be found in Fig. 1. The propagation loss of the HIC SDS waveguide is below 0.1 dB/cm, and $\mathrm{MFD}_{x\times y} = 1.6 \times 1.7$ μm. The effective index and group index for the TE_{00} mode at 1.55 μm wavelength are 1.535 and 1.72, *resp*. A minimum bending radius of 100 μm is feasible, based on the criterion that bend losses should be below 0.01 dB/cm [14].

By vertically tapering the thickness of both Si_3N_4 layers from 170 nm down to 35 nm near the end-facets, while the intermediate SiO_2 layer thickness is kept constant at 500 nm, allows for a spot-size converter (SSC) for low-loss fiber-to-chip coupling to standard telecom glass fibers with a MFD of 10 μm: fiber-to-chip coupling losses from SMF28 single-mode fiber to the LIC SDS waveguide below 0.5 dB/facet have been achieved.

D. Asymmetric Double-Stripe or ADS

The asymmetric double-stripe (ADS) has a similar waveguide geometry to the SDS: the main difference is that the thickness of the upper Si_3N_4 stripe is different than the lower Si_3N_4 stripe, see Fig. 2 for a schematic cross-section, while also the thickness of the intermediate SiO_2 layer is significantly smaller: instead of 500 nm as for the SDS geometry, a thickness of 100 nm is used for the ADS geometry. The lower Si_3N_4 layer of the ADS geometry allows for optimization of coupling to external components such as fibers and/or active materials without adjusting its thickness, while the upper Si_3N_4 stripe thickness can be optimized for a target bending radius and is removed completely (tapered down to zero thickness) elsewhere in the circuit. The thickness for the upper Si_3N_4 stripe of 175 nm has been chosen to give the HIC ADS geometry the same effective index of 1.535, the same minimum bending radius of 100 μm as the HIC SDS geometry. Please note that the group index is not the same as for the SDS waveguide: the ADS waveguide has a slightly larger group index of 1.77. The mode-field size is $\mathrm{MFD}_{x\times y} = 1.5 \times 1.2$ μm which is also different than for the SDS waveguide (especially in vertical direction the ADS mode field is more compact). Compared to the SDS geometry, the ADS geometry requires less fabrication steps, going with higher yield and even better optical characteristics. Propagation loss values on ADS waveguides are reproducibly measured to show similar or better values compared to SDS waveguides, so $<$0.1 dB/cm The ADS propagation losses are expected to be reduced further to values close to 0.01 dB/cm.

The complete removal of the thick top layer of Si_3N_4 allows for a "natural" transition from the LIC ADS to the HIC ADS waveguides, which -in turn- makes it possible to combine the potentially ultra-low-loss properties of the single-stripe geometry with the small bending radii of the HIC ADS geometry, by placing a spot-size converter in between (for more discussion on this topic, see Section III-C).

Table II gives an overview of the most important properties of the different TriPleX geometries discussed in this Section. The

TABLE II
OVERVIEW OF THE MOST IMPORTANT PROPERTIES OF THE DIFFERENT TRIPLEX WAVEGUIDE GEOMETRIES

WG type	Box shell		Single-stripe	Symmetric double-stripe		Asymmetric double-stripe	
Stack ($t_{Si3N4}/t_{SiO2}/t_{Si3N4}$)	HIC BOX 170/500/170	LIC BOX 50/1000/50	$t_{Si3N4} = 65$	HIC SDS 170/500/170	LIC SDS 35/500/35	HIC ADS 70/100/175	LIC ADS 75/100/0
λ [nm]	1550	1550	1550	1550	1550	1550	1550
mode	TE_{00}	TE_{00}	TE_{00}	TE_{00}	TE_{00}	TE_{00}	TE_{00}
w [μm]	0.84	1.1	4.2	1.2	1.0	1.1	0.8
w_{SMB} [μm]	0.8	2.8	4.2	1.5	4.5	1.4	3.7
MFD_x [μm]	1.4	3.6	4.7	1.6	10	1.5	10
MFD_y [μm]	1.4	3.6	2.9	1.7	10	1.2	10
R_{min} [μm]	150	500	2000	100	∞	100	∞
N_{eff}	1.555	1.455	1.459	1.535	1.447	1.535	1.446
N_g	1.76	1.49	1.50	1.72	1.46	1.77	1.46
α_{prop} [dB/cm]			≤0.03	≤0.1		≤0.1	

design wavelength λ and mode are given, the waveguide width w. The parameter w_{smb} is the waveguide width at the single-mode boundary, $MFD_{x,y}$ are mode-field diameters where the optical power has dropped to 1/e² of the maximum intensity, R_{min} is the minimum bend radius, where the bend losses are below 0.01 dB/cm, N_{eff} is the effective index, N_g is the group index, and α_{prop} is the waveguide propagation loss.

E. Manufacturing Process of the Basic TriPleX Geometries

The general process flow is illustrated schematically in Table III for the production of the different basic TriPleX geometries. The left-hand column shows the production process for the box shell, the right-hand column is related to the other geometries, the double-stripe SDS and ADS. The scheme for single-stripe is nearly the same as for the double-stripe geometries, except that step 4 and 5 can be skipped then.

The applied deposition techniques are the result of many years of production optimization and characterization. The current scheme contains as many batch processes as possible, using equipment that is present in most CMOS foundries: this makes production of TriPleX waveguides suitable for mass production. At the same time the optical properties also have been optimized. The highest quality SiO_2 layer results from wet thermal oxidation of single-crystal silicon substrates to create an SiO_2 layer (Table III, steps 1, 2), typically at temperatures equal to or above 1000 °C. As discussed earlier in Section II-B, the lowest reported propagation losses have been achieved using a bonded thermally grown SiO_2 layer as top cladding.

Low-pressure chemical vapor deposition (LPCVD) is used for the Si_3N_4 layers and, where thermal oxidation is not applicable, also for the SiO_2 layer. For the latter process, the gas tetraethylorthosilicate (TEOS) is used. LPCVD deposition results in high quality layers, shows very good layer uniformity, both in thickness and in refractive index, good step coverage because of conformal growth, and the layer is deposited on both sides of the substrate at the same time (Table III, step 3, 4, 5, 7, and 9) [15], [16].

Drawback of this technology is the limited layer thickness: for Si_3N_4, the critical layer thickness is in the order of 300 nm, for SiO_2 the critical layer thickness is about 1500 nm. Above the critical layer thickness, cracks will occur, caused by the internal stress due to differences in coefficient of thermal expansion (CTE) between the deposited layer and the silicon substrate. However, the stress of Si_3N_4 films on Si is tensile, while SiO_2 films on Si are compressive: alternating stacks of oxide and nitride therefore show reduced macroscopic stress values, and consequently allow for more nitride incorporated in the waveguide. This forms the basis for the patented TriPleX technology.

As typical top cladding thicknesses of at least 8 μm cannot easily be achieved if only LPCVD TEOS SiO_2 is being deposited, a part of the top cladding is deposited using another deposition technique: plasma-enhanced chemical vapor deposition (PECVD). Typical deposition temperatures are between 300 °C and 400 °C. This growth technique is directional, and as the substrate has to lie down on a bottom electrode (for the generation of the plasma), this type of film is deposited on one side of the substrate. The stress in PECVD SiO_2 layers (Table III, step 10) is much less than in LPCVD layers, allowing for much thicker layers.

Besides the optical quality and the surface roughness of the used deposition techniques, another factor that is important for low-loss propagation of light is the sidewall roughness or line edge roughness (LER), which is determined by the details of the photolithographic process and the etching technique that is used for the waveguide definition (Table III, steps 6, 8) [4].

III. BASIC BUILDING BLOCKS (BASIC STRUCTURES & FUNCTIONALITIES)

TriPleX waveguide technology in principle is passive, as it is not (yet) possible to monolithically integrate light sources, electro-optical modulators, or detectors with competing specifications. However, to be able to tune optical properties of integrated optical (IO) devices, thermo-optical tuning can be achieved by means of resistive metal-based heaters on the top cladding [17], [Section III-E], stress-optical tuning is possible by integration of PZT piezoelectric devices on top of the top cladding [18], [Section III-F], and electro-optical tuning can be realized by locally defining sensing windows through the top cladding until near the guiding layer that are filled with a liquid

TABLE III
GENERIC PROCESS FLOW FOR THE FABRICATION OF THE BASIC TRIPLEX GEOMETRIES [4]

TriPleX box shell	*TriPleX SDS, ADS*	*TriPleX box shell*	*TriPleX SDS, ADS*
1. Silicon substrate		*6. Waveguide patterning after etch and resist removal*	
2. SiO_2 bottom cladding by wet oxidation		*7. Si_3N_4 layer by LPCVD*	N/A
3. Si_3N_4 layer by LPCVD		*8. Local removal of Si_3N_4 layer*	N/A
4. SiO_2 intermediate layer by LPCVD TEOS		*9. SiO_2 top cladding layer by LPCVD TEOS*	
5. Si_3N_4 layer by LPCVD		*10. SiO_2 top cladding layer by PECVD*	
N/A			

crystal, and by generation of an electric field across the liquid crystal [19], [20].

In this section, an overview is given of the basic building blocks that are also available through MPW runs [11], [12], [13].

A. Routing Building Blocks

The most elementary basic building blocks are routing building blocks, that are based on regular straight waveguide building blocks (either with constant width or with varying width for lateral tapers), and on polar bend building blocks (based on bends with constant radius of curvature). Based on these building blocks, more advanced routing building blocks can be defined, such as S-shaped bends. Furthermore, transition losses between different routing elements due to a lateral offset in the position of maximum light intensity (caused by a difference in radius of curvature) can be solved geometrically in two ways: either by introducing a lateral offset at the junction between the elements to avoid discontinuity in the position of maximum light intensity, or by designing a different type of bend shape that adiabatically changes the radius of curvature such as e.g., a (co)sine-shaped bend.

B. Spot-Size Converters

SSCs modify the MFD of a waveguide either by using a vertical taper, as discussed in Section II-C, and/or by changing the waveguide width using a lateral taper. The vertical taper can be designed to locally and adiabatically change the thickness of the guiding layer(s) such that discontinuities in MFD are avoided, to minimize the excess loss of the SSC, at the cost of a length of typically several hundreds of μm. The SSC can be used to minimize coupling loss to e.g., a glass fiber, where the end-facet waveguide typically has a 90° angle, as the effective index of TriPleX waveguides are quite close to that of standard glass fibers for telecom). Another application is coupling to a waveguide from another integrated optical chip such as light sources manufactured in InP technology. Because of the much larger effective index of waveguides in other technologies such as InP, SOI, the SSC coupling loss can be decreased by placing it under a suitable angle different than 90°, more can be found in Section VI-A.

C. Splitters/Combiners and Couplers

To split light in a waveguide into two or more branches (or to combine light from two waveguides into one branch), a Y-junction is an interesting option, as the splitting (or combining) ratio is theoretically 50% and wavelength- and polarization-independent. However, to make the Y-junction splitting ratio robust against technological variations, a certain minimum gap between the two branches has to be taken into account. The extra robustness is at the penalty of additional excess loss (sub-dB level), which is also wavelength- and polarization-dependent.

If lower excess loss is required, a directional coupler (DC) is more interesting, if one can tolerate the wavelength- and polarization-dependency of the coupling ratio. The excess loss of a DC, opposed to a Y-junction, is not dependent on wavelength. The coupling ratio is determined by both the gap between the two branches and the coupling length, which makes the DC more versatile than the Y-junction which is limited to 50% splitting ratio.

A more versatile splitter/combiner is the multi-mode interferometer (MMI) and a more generic coupler is the star coupler (SC), both of which can be designed as $M \times N$ devices. More complex building blocks such as arrayed-waveguide gratings (AWGs) are typically based on such $M \times N$ devices. However, if one has to deal with only a few waveguides, it could be that (a cascade of) Y-junctions or DCs have more interesting specifications, because the MMI and the SC have a wavelength- and polarization-dependent excess loss.

D. Phase Modulators

The phase modulator that is standardly used for the examples in this paper is based on thermo-optical tuning by means of heaters on top of the top cladding above a waveguide. These are manufactured by defining structured metal patterns based on a chromium layer and a gold layer. The gold layer is removed locally where the heat has to be generated, and from the traces that are covered with gold for efficient transport of electrical current to the heater. By combining e.g., two Y-junctions and two straight waveguides, one with a phase modulator and the other without, one can define a tunable coupler based on a Mach-Zehnder interferometer (MZI).

Thermo-optic actuators on TriPleX are reliable, straightforward to manufacture, and offer tuning speeds around 1 ms. However, thermo-optic actuators suffer from power dissipation, in the order of 300 mW per π phase-shift per modulator, and thermal cross-talk from neighboring heaters requires a distance of at least 250 μm to the nearest neighboring waveguide. While their tuning speed is sufficient to drive applications such as beamforming matrices and programmable photonic processors, the constant power dissipation of thermo-optic actuators makes them inappropriate to support large scale waveguide-based matrices. For these reasons, alternative types of phase modulators have been developed, as is mentioned in the first paragraph of Section III, namely stress-optic modulators (see the next section).

E. Stress-Optic Actuator

To drastically decrease the power dissipation, ultra-low-power stress-optic phase actuators are implemented in the TriPleX platform for visible light [18] as well as for the telecommunication C-band [21]. In these stress-optic actuators, the stress is induced into the waveguide by a piezoelectric PZT (lead zirconate titanate) layer, which is actuated by applying a voltage at an electrode. When the PZT on top of the waveguide is exposed to an electric field, the PZT expands in the direction along the electric field while simultaneously contracting in the two other directions resulting in stress in the waveguide structure.

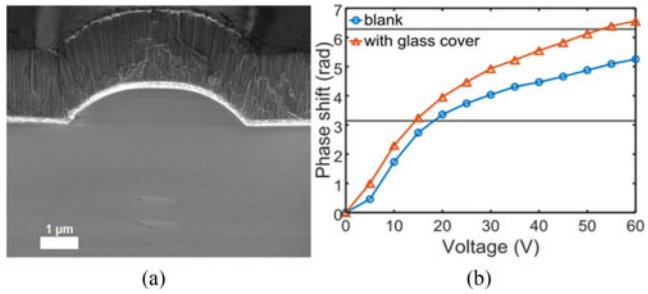

Fig. 3. (a) SEM picture of the stress-optic actuator. (b) Phase shift as a function of applied voltage for a top electrode (length of 14.8 mm and width of 5 μm) with (orange triangles) and without a supportive glass cover (blue circles).

Fig. 3 shows a scanning electrode microscope (SEM) picture of the cross-section of a stress-optic actuator for the C-band. For actuators in the C-band the efficiency of the actuator is optimized by, amongst others, focusing the applied stress in the waveguide core region through a local increase of the top cladding. The stress-optic actuators were fabricated using a symmetric double stripe TriPleX geometry (see Section II-C). Afterwards a bottom electrode consisting of a 10 nm thick titanium adhesive layer and a 100 nm thick platinum layer was deposited. The PZT layer with a thickness 2 μm was grown using pulsed laser deposition allowing for the growth of high-quality layers on large wafer sizes and at commercial throughput [22]. Finally, platinum top electrodes with a thickness of 100 nm were deposited. Using a Mach-Zehnder interferometer, a half-wave voltage, V_π was measured at 18 V at a wavelength of 1550 nm using an actuator with a top electrode width of 5 μm and an actuator length of 14.8 mm as shown in Fig. 3(b). The performance of actuator can even be further improved by a supportive glass cover plate on top of the actuator. The improved actuator showed a V_π of 14.5 V and even a phase tuning of 2π at 50 V without applying any bias voltage.

The measured static power consumption of the stress-optic phase actuator is in the μW-region as it is only determined by small leakage currents ($<$0.1 μA), which could not be measured in experiment. While the dynamic power consumption at a rise time of 1 ms (1 kHz excitation) is calculated to be less than 1 mW per actuator for an actuator capacitance of 3 nF. This makes the stress-optic actuator at least 1000 times more power efficient than thermo-optic tuners in the static case and more than 300 times at 1 ms rise time.

To ensure the ultra-low loss characteristics of TriPleX waveguides, it is important to choose a sufficiently thick silica top cladding to prevent excess losses introduced by the Pt bottom electrode. The TriPleX stress-optic actuator goes with a calculated excess loss of less than 0.01 dB per actuator only.

IV. Basic Functionalities

A. Ring Resonator Filter

An important functionality that can be realized with low loss TriPleX waveguide is optical filtering via micro-ring resonators

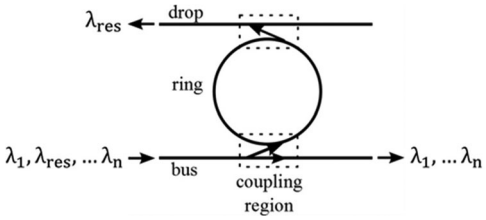

Fig. 4. Schematic of an add-drop ring resonator filter. When approaching the coupling region, only if the input wavelength is in resonance with the optical resonator length, the light couples into the resonator and is dropped out to the upper waveguide.

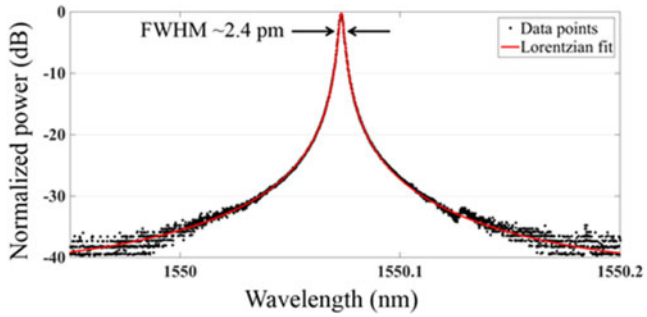

Fig. 5. Transmission spectrum of a single resonance peak of an add-drop ring resonator. A Lorentzian fit is performed and a full-width-at-half-maximum of ~2.4 pm is obtained. This corresponds to a quality factor Q ~ 700 thousand.

(MRRs). Such MMRs have been shown to be very important and useful for many applications such as optical delay lines [23] enabling optical beam-forming networks [24], bio-sensing [25] and many non-linear processes [26].

A first-order ring resonator filter is composed, in an add-drop configuration, by a waveguide closed on itself (having a ring topology) and two straight waveguides (bus and drop) coupled together (Fig. 4).

When light in the bus waveguide approaches the coupling region it will or won't tunnel into the ring, depending on whether it's wavelength is resonant with the optical cavity length. The ring waveguide behaves thus as a wavelength selective optical cavity that stores, enhances and drops out only resonant light, while all other light is transmitted to the output.

The cavity life-time determines the optical filtering bandwidth where a longer cavity life-time corresponds to a narrower filtering bandwidth. The life-time of the cavity, that determines the Q-factor of the resonator, is heavily affected by the internal losses. In order to increase the cavity life-time and Q-factor, the internal losses of the cavity, of which propagation loss is a main contribution, need to be substantially reduced. The TriPleX technology is able to provide an optimized combination of straight-propagation loss and curvature loss via selecting an appropriate cross-section (Section II) [8]. Thereby, high-Q-factor ring resonators can be fabricated within a standard and well-reproducible fabrication process. In Fig. 5 we report the measured transmission spectrum of a single resonance of an add-drop ring resonator filter which shows a Q-factor $\sim$700 thousand, as achieved with standard fabrication. From the Q-factor it is possible to derive the value of the propagation losses which are, in the case presented in Fig. 2, as low as 0.07 dB/cm. The add-drop ring resonator is fabricated with a single stripe cross-section of 2.5 um width and 250 nm thickness, and with a radius of 365 μm. As discussed previously (Section II-B) the described dimensions of a single stripe cross-section enable the lowest propagation loss, compared to the other cross-sections, at the given radius of the resonator.

Such a high Q-factor is well desirable for applications as high-resolution on-chip spectrometers and for nonlinear conversion [27]. One example would be optical parametric oscillation and comb generation. We calculated the threshold power [28] for which we used the Q-factor given in Fig. 5 and the resonator length of 3400 μm. However, because the confinement is only moderate with a mode field area of about $10\,\mu\mathrm{m}^2$, the gain is mainly due to the lower nonlinear index of the SiO_2 cladding [29], and the mode volume is relatively large. This yields a threshold in the order of 10 W, and due to normal dispersion the spectral coverage would remain closely around the pump wavelength. A wide spectral coverage of hundreds of THz can be obtained with dispersion engineering via tight confinement to about 1 $\mu\mathrm{m}^2$ mode area [30], [31]. In spite of increased losses (0.37 dB/cm [32]), the much larger nonlinear index of the Si_3N_4 core can be accessed (see [30] and refs. therein), and the mode volume can be significantly reduced. For a resonator radius of 320 μm and 0.5% coupling we calculate a threshold of about 100 mW, which is well comparable with previous experimental data based on similar material [33]. Of high interest is bringing the threshold further down into the range that is accessible to on-chip lasers as described in Section VI.

B. Mach-Zehnder Filter

An addition to the ring resonator-based wavelength filters are Mach-Zehnder filters (MZFs). Especially for a large free spectral range (FSR), an MZF can be build where ring resonator-based filters are limited by bending loss (see Section II). Fig. 6(a) shows the schematic of an MZF, where the incoming light is split by a directional coupler into two arms with a path lengths difference, ΔL, and combined again using a second coupler. Ideally, the spectral response (transmission spectrum) of an MZF is, a sinusoidal function where the FSR is given by: $\mathrm{f_{FSR}} = \mathrm{c}/(\mathrm{n_g}\Delta\mathrm{L})$, where c is the speed of light and $\mathrm{n_g}$ is the group index.

An example of the spectral response of an MZF is shown Fig. 6(b). Here an MZF was actuated using a stress-optic actuator with an electrode length of 1.5 cm and a ΔL between the two arms of 100 μm resulting in an FSR of 14.5 nm (see Section II-F). The highest obtained suppression ratio was more than 30 dB, while suppression ratios for individual wavelengths differ due to the wavelength dependence of the directional coupler. If properly designed, MZFs can be realized to be versatile wavelength filters in both suppression ratio and FSR. Furthermore, higher-order filters can be realized to achieve flat-top filter response [14].

C. Ring Resonator Based Delay Lines

Tunable delay lines are essential building blocks for implementing optical signal processing functions on chips. In particular, microwave photonic applications like optical beamforming

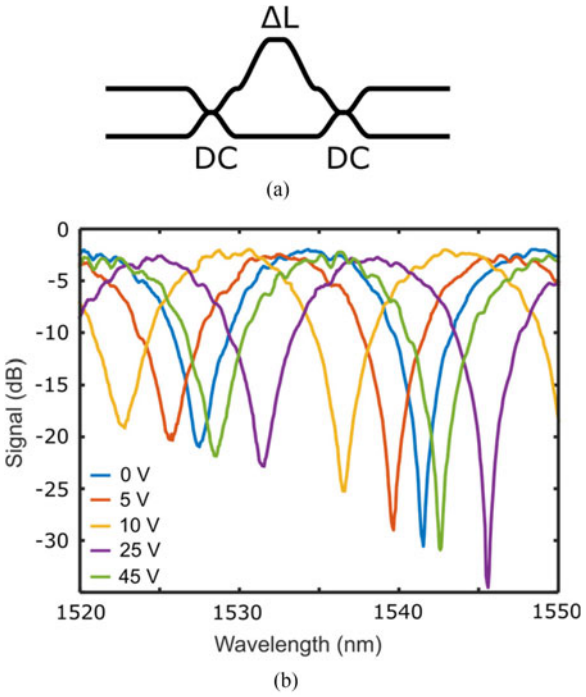

Fig. 6. (a) Schematic of a Mach-Zehnder filter; DC: directional coupler. (b) Spectral response of a Mach-Zehnder filter based on stress-optic actuation for various voltages. The filter has a path difference of 100 μm between its two arms resulting in a free-spectral-range of 14.5 nm.

networks for phased array antennas with physical apertures in the order of tens of cm or larger and highly-selective spectral filters with MHz-level frequency resolution need many and long delays on one chip. In accordance, these delays must be in the same order of length, i.e., tens of cm or larger (equivalently multiple nanoseconds in time), and therefore low-loss waveguide is an essential requirement for the implementation.

TriPleX waveguides provide a path for practical solutions, where ring resonators are used comprising tunable phase shifts in the ring loops and tunable couplers. The conventional ring resonator delay lines use identical ring resonators, which have a frequency-periodic delay response. This means that when used for multi-λ based tapped-delay-line filters, in general, each λ will require an independent delay line to generate the different delays of the filter taps. This gives rise to circuit complexity issues for filters with a large number of taps. An alternative approach to address this issue is to create delay lines that are able to simultaneously provide multiple different delays at different wavelengths or optical carrier frequencies. We proposed and experimentally demonstrated such delay lines using the Vernier configurations of ring resonators [34], namely combining ring resonators of different FSRs. Two types of Vernier configurations were considered as shown in Fig. 7, i.e., the serial cascade (referred to as delay line A) and coupled configurations (referred to as delay line B), where the former features easier control (as each ring resonator is independent from the others) and the latter less chip area (as B uses about half the footprint size as compared to A). The core concept here is to implement multiple different delays staggered in frequency. In principle, a combination of ring resonators with N different FSRs allows for the

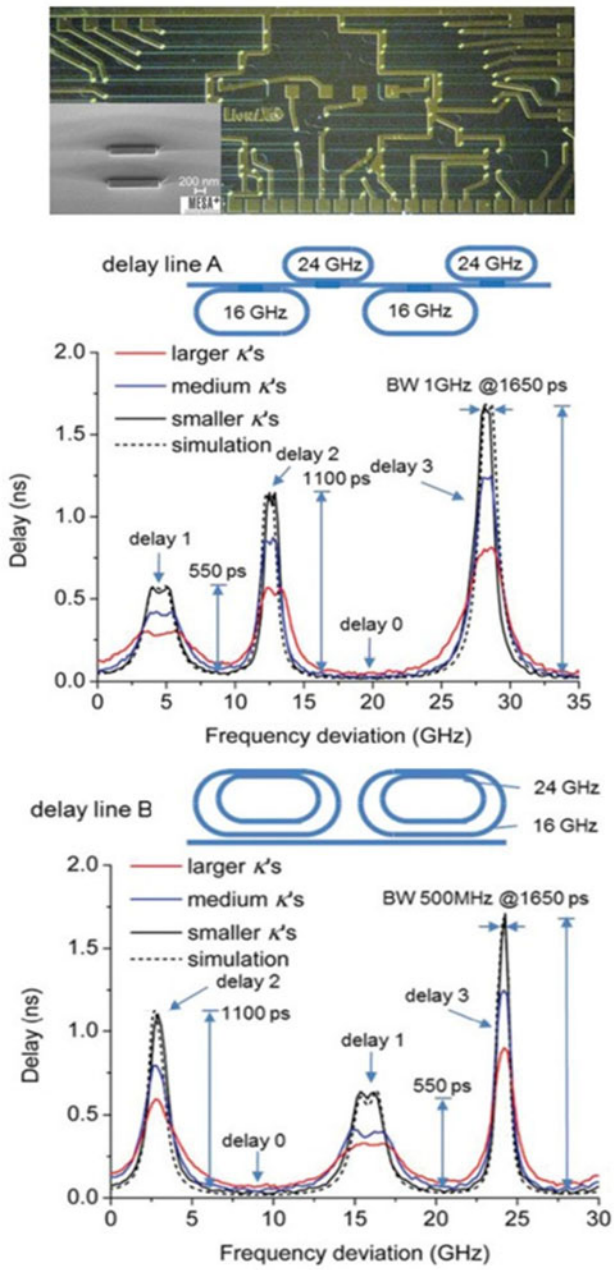

Fig. 7. A photo and schematics of two Vernier configurations of ring resonators as delay lines implemented using TriPleX waveguide, associated with measurements of different delays tuned via ring resonator coupler coefficient κ, which are in agreement with the theoretical calculations.

simultaneous generation of 2N-1 different delays per frequency period. This can be employed in multi-λ schemes of tapped-delay-line filters to significantly reduce the system complexity. In the experiment, an inter-delay step of 550 ps and a maximum delay of 1650 ps for a bandwidth of 500 MHz were achieved using 4-ring Vernier configurations with ring resonators having FSRs of 16 GHz and 24 GHz, as shown in Fig. 7.

D. AWG Based Wavelength Independent Switch

To switch ~100 nm broadband light between multiple fiber outputs, without any moving parts, a wavelength independent optical switch with 3 inputs and 80 outputs was designed and

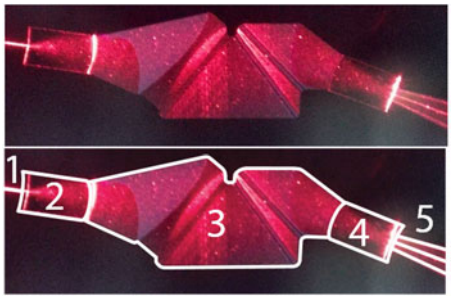

Fig. 8. (Top) Photograph of a 3-to-80 port AWG, with red light, only used for illustrative purposes, inserted in a single waveguide. Output shows three outputs instead of one, because of higher order spatial modes. (bottom) Legend of the AWG, where 1 indicates the input waveguide, 2 indicates a multimode interferometer (MMI), 3 indicates the dispersive part of the AWG with 103 waveguides, 4 indicates the output-side MMI and 5 indicates the output waveguides.

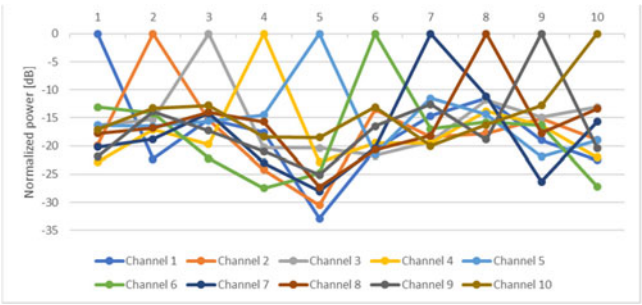

Fig. 9. Switching between 10 different output ports of the AWG, while measuring the output power of all 10 ports simultaneously. In this measurement, a typical cross-talk suppression of >12 dB per waveguide is shown.

fabricated by using a so-called zero-order AWG. Contrary to other AWGs, a zero-order AWG is wavelength independent. By adding tuning elements, such as heaters, on the arms of the AWG it acts as a wavelength independent switch. As example, in Fig. 8(a) zero-order AWG design is shown, containing 3 inputs, 103 arms and 80 output waveguides without tuning elements with red light coupled into the waveguide. The design is developed for a wavelength range from 1530 nm to 1565 nm.

For a wavelength of 660 nm, only used for illustrative purposes, the higher order spatial modes are present in the outer waveguide outputs, causing multiple outputs (three in this case). A similar AWG has been measured where tuning elements were added onto the waveguide arms, such that they can be tuned from 0 to 2π individually. By tuning the individual tuning elements, the output port can be switched and the suppression of the other output ports can be optimized. This building block can be designed for many required output numbers.

As example, we show switching between 10 output waveguides in Fig. 9. From this measurement, it is clear that a high suppression can be achieved with optimizing the AWG settings. A suppression of >12 dB for each waveguide was measured, i.e., if optimized for output at a single waveguide, a maximum of -12 dB was measured (compared to the optimized waveguide) at any of the other AWG output waveguides. Measurements on the insertion loss of such an AWG around a wavelength of 1550 nm, optimized for maximum output power in a single waveguide, indicate that the insertion loss of the used AWG is less than 2 dB.

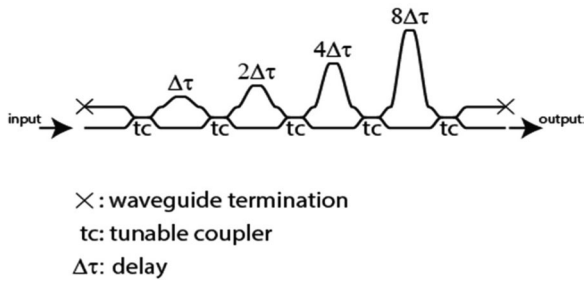

Fig. 10. Schematic overview switched delay line.

V. COMPLEX FUNCTIONALITIES

A. Switched Delay Line

Switched delay lines are commonly used in OBFNs, signal processers, signal routers and buffering [35]. An example of an OBFN with continuously variable delays is discussed in Section VI-C. This section focuses on a delay line with discrete delay steps. It is clear that for large delays, low loss waveguides offer advantages in the difference between propagation losses for different delay-line settings (called dynamic loss), as well as absolute loss of the delay line (insertion loss). To demonstrate this, a 4-bit switched delay with tunable couplers (TC) between the different delay lines has been designed and fabricated. The schematic layout is shown in Fig. 10. The delay targets for the fabricated 4 bits were, respectively, $\Delta\tau = 3.2$ ps, $2\Delta\tau = 6.5$ ps, $4\Delta\tau = 13$ ps and $8\Delta\tau = 26$ ps.

For statistics, 13 individual delay lines were measured, with thermal-optical based TCs. As the average consumed power per TC is $\sim$0.3 W, the average power consumption of the switched delay line is $\sim$1.5 W. The optical cross talk, being the light travelling through an unwanted delay path interfering with the wanted delay path, is twice the amount of optical suppression of a tunable coupler. This results from design, where from input to output the light goes at least through two TCs in cross state. Typical values for the suppression were between 15 to 25 dB, leading to an optical cross talk lower than -30 to -50 dB. The measured delay values are shown in Fig. 11, where the dashed lines indicate the target delays (as mentioned above) and the different dots indicate the measured delays (each dot per delay corresponds to a different delay line) and the blue line indicates the trend, which is as expected a linear line. The absolute difference per delay, which we call the delay error, is smaller than ± 0.5 ps, as is shown in Fig. 12, where each dot indicates a separate measurement. The measured switching time was less than 0.4 ms. As is clear from these measurements, low-loss TriPleX is very suitable for fabricating switched delay lines.

B. Reconfigurable Photonic RF Filter

Photonic implementation of RF filters enables unprecedented features in terms of bandwidth, tunability, and ability to integrate with other signal processing functions in the optical domain.

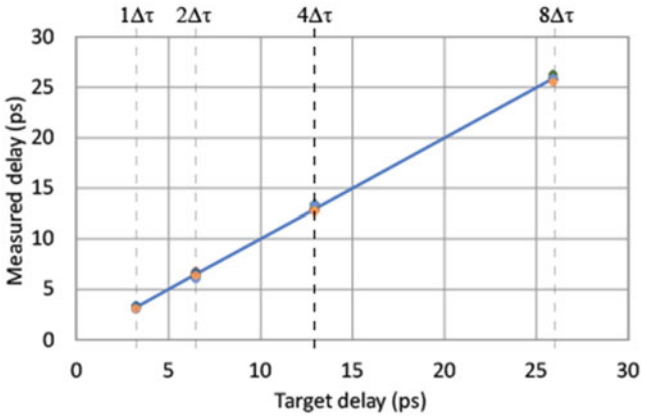

Fig. 11. Measured delays of 13 individual 4-bit switched delay lines. The measured delay is plotted as function of the target delay. The solid straight line (blue) intersects the target delays.

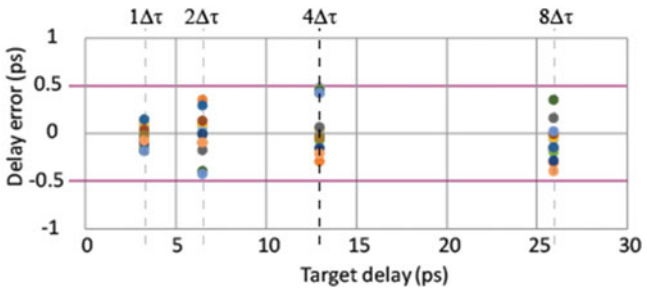

Fig. 12. Measured error per targeted delay value for the 13 individual 4-bit switched delay lines. Each dot indicates a separate measurement.

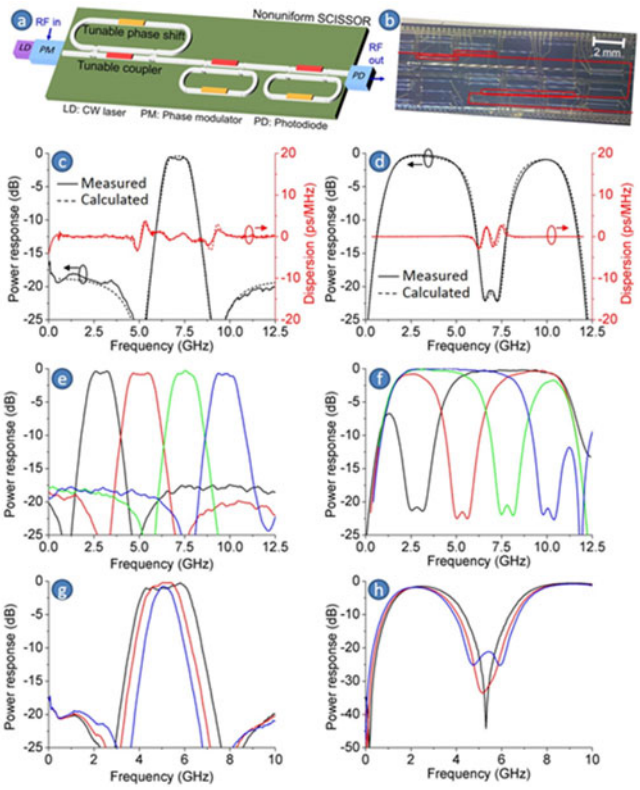

Fig. 13. (a) A schematic of an integrated microwave photonic implementation of a RF filter using a nonuniform 3-ring SCISSOR. (b) A photograph of a fabricated test chip with indications of the ring resonators. Experimental demonstrations of (c), (d) the bandpass and bandstop RF filter shapes, (e), (f) the tuning of filter center frequency, and (g), (h) the varying of bandwidth.

However, from a practical perspective, the filter performance is highly dependent on the optical losses as most implementations have the eventual RF-to-RF insertion loss in quadratic relation with the optical losses due to the square-law effects of the optoelectronics used therein. For this reason, TriPleX appears to be a very promising platform for RF applications. Next to this, another key feature for the filter design is the filter shape reconfigurability as it significantly broadens the potential for application of a filter. Besides, having an entire filter fully integrated on a unit provides the ultimate system stability, control precision, and device compactness. In this context, a highly reconfigurable photonic RF filter is proposed which comprises a serial cascade of three of silicon nitride ring resonators [36]. In the experimental demonstration, double sideband modulation is employed, which can be easily implemented using an intensity or phase modulator.

Regarding the ring resonators, a pair of identical ring resonators are used for filter shape synthesis and a third ring resonator with a smaller FSR is used to perform the function as modulation transformer [37] that enables a separate manipulation of the phase of the optical carrier. Then, through optical detection, a RF filter with a nearly DSP-level of shape reconfigurability is implemented, as shown in Fig. 13. All the reconfiguration operations including filter frequency tuning, bandwidth variation, and switching between band-pass and band-stop filter shapes are implemented using the tuning mechanism on the ring resonators.

C. High-Granularity WDM Filter

TriPleX circuits also promise a significant impact on the next generation elastic optical communication networks, where technologies enabling high spectral efficiency and fine granularity transmissions are of significant use to increase the network capacity and flexibility. One reason for this is that the low-loss feature of the waveguide supports designs of filter structures with long delay paths, e.g., multiple cm, and therefore enables spectral processing with resolution finer than 1 GHz, which in contrast is challenging to implement using free-space optics. One interesting function is a Nyquist-filtering (de)interleaver [38] implemented using a ring resonator-assisted Mach-Zehnder interferometer (RAMZI) circuit that comprises an asymmetric MZI with each arm coupled with a ring resonator as shown in Fig. 14.

The design presented here employs a total of seven tuning elements, i.e., two tunable couplers at the input and output of the MZI, two tunable couplers of the two ring resonators, and three tunable phase shifters in the ring loops and MZI delay line. This concept has been experimentally demonstrated using a RAMZI with an interleaver period (FSR) of 25 GHz and a 3 dB passband bandwidth of 12.5 GHz as shown in Fig. 14. The RAMZI is used

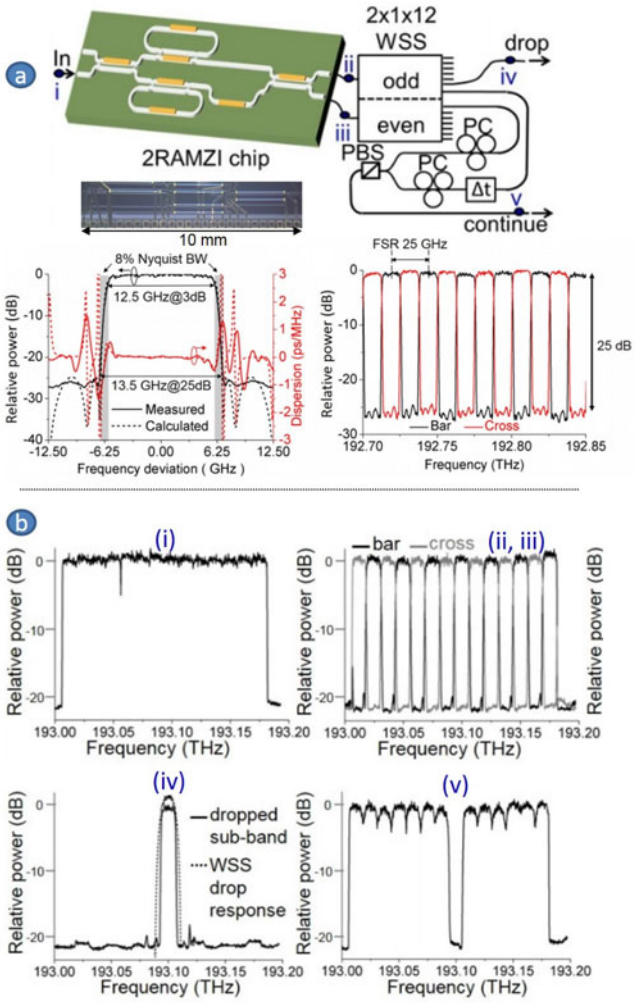

Fig. 14. (a) Design and (b) spectral filtering of a reconfigurable RAMZI circuit as a Nyquist-filtering interleaver for WDM superchannel demultiplexing.

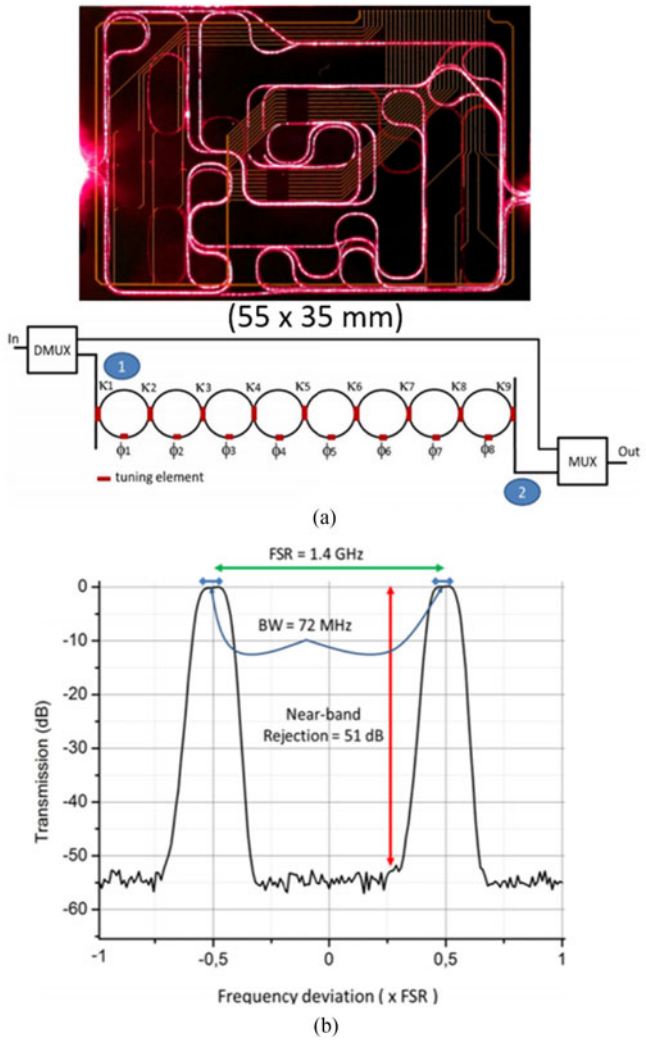

Fig. 15. (a) Picture and layout of the fabricated high order filter in TriPleX, and (b) Measured transmission response of the fabricated MWP filter.

as a pre-deinterleaving stage in combination with a commercial wavelength selective switch (WSS) to implement a resolution-enhanced WSS. Using this combination, a WDM superchannel ROADM was enabled, which supports a sub-channel spacing of 12.5 GHz, a factor of four smaller than the current 50 GHz DWDM grid.

D. High-Order Ring Resonators

Another interesting application of high-order ring resonators is input and output multiplexers (IMUXs and OMUXs) of satellite transponders in the field of satellite communications. These functions have stringent requirements for filter selectivity, typically in the order of MHz. As these devices are to be space borne or airborne they need to be small in size and weight, and simultaneously provide low power consumption (SWaP). Currently, the implementation of these functions relies on bulky electronics.

However, microwave photonics using TriPleX waveguide opens an alternative solution. For example, a Ku-band IMUX requires a channel bandwidth ranging from 27 MHz to 95 MHz for the frequency band from 10.7 GHz to 12.75 GHz. Fig. 15 shows an example of such a circuit which comprises an optical carrier-sideband demultiplexer and a multiplexer with a highly frequency-selective optical filter in between [39]. The optical filter is an 8th-order coupled ring resonator network, whose layout and picture are presented in Fig. 15(a) with an FSR of 1.4 GHz and has tunable couplers and tunable phase shifters in all ring loops.

By properly configuring these tuning elements, a remarkable filter performance was experimentally demonstrated, i.e., a 3 dB passband of 72 MHz, a −30-dB bandwidth of about 140 MHz, and a stopband rejection of 51 dB, while maintaining a very low filter insertion loss (excluding fiber-chip coupling losses) of <6 dB. As an important milestone of the waveguide technology, this filter shows an excellent combination of frequency selectivity, power rejection, and insertion loss when using the longest waveguides that were ever applied in such filters, i.e., each ring loop having an optical length of 21 cm. A single pass through all resonators thus corresponds to about 1.7 m, and taking into account that multiple roundtrips are performed in the

resonators, the effective optical path length amounts to several meters. It is important to highlight that realizing such a filter in a chip-format has been possible only because of the very low waveguide loss, measured as low as 1.4 dB/m, provided by the single stripe waveguide presented in Section II-B.

E. Programmable Photonic Integrated Circuits for General Purpose Optical Processor Chip

Integrated optical signal processors promise a wide range of applications in several different fields including optical communication networks, microwave photonics, optical sensing, biophotonics, and quantum optics. Conventional solutions use the so-called application-specific photonic integrated circuits (ASPICs), in which each is designed to perform a particular function. In practice, this paradigm may have issues of cost and flexibility, which are determining factors from a commercial perspective. A radically different approach in contrast to ASPICs is so-called programmable optical chips [40], i.e., universal signal processors integrated on optical chips. By programming such a processor suitably, it is possible to implement different functions as desired. This is a similar concept as digital signal processors and field-programmable gate arrays (FPGAs) in microelectronics, where, through a software-defined approach, common hardware is shared for multiple functionalities. A first design of such a programmable optical signal processor chip has been proposed [41] and experimentally demonstrated. The chip comprises several identical Mach-Zehnder couplers that are interconnected in the topology of a two-dimensional lattice mesh network as shown in Fig. 16. The Mach-Zehnder couplers have their both arms equipped with phase tuning elements. This design allows each Mach-Zehnder coupler to be configured to perform either a 2×2 coupler or an optical path routing switch, with the capability of simultaneously controlling the optical amplitude and phase, and therewith serving as a basic programmable unit. In principle, when provided with a sufficiently large network scale, one can program those Mach-Zehnder couplers to implement an arbitrary interferometric circuit topology for signal processing purposes, e.g., FIR and IIR filters, with full control of circuit parameters (amplitude and phase of each optical path in the circuit). It is worth mentioning that in principle such a chip on its own would be able to implement all the optical processing functions described in this works and beyond, implying a remarkable potential for applications and commercial prospect of TriPleX platform. However, as the network size scales up, waveguide loss plays an increasingly significant role for the device performance. In return, this would provide a strong motivation for the further development of the waveguide and therewith establish a key benefit of TriPleX platform. Moreover, such processors also allow for implementations of a multi-port switch network or a bank of parallel signal processing functions.

F. All-Optimized Integrated MWP Notch Filter

Microwave photonics (MWP) is an emerging technology of which photonic technologies are used to generate, distribute, process, and measure RF and microwave signals [42]. Recently, there is a strong paradigm shift towards the incorporation of photonic circuits in MWP leading to integrated MWP devices and systems [43].

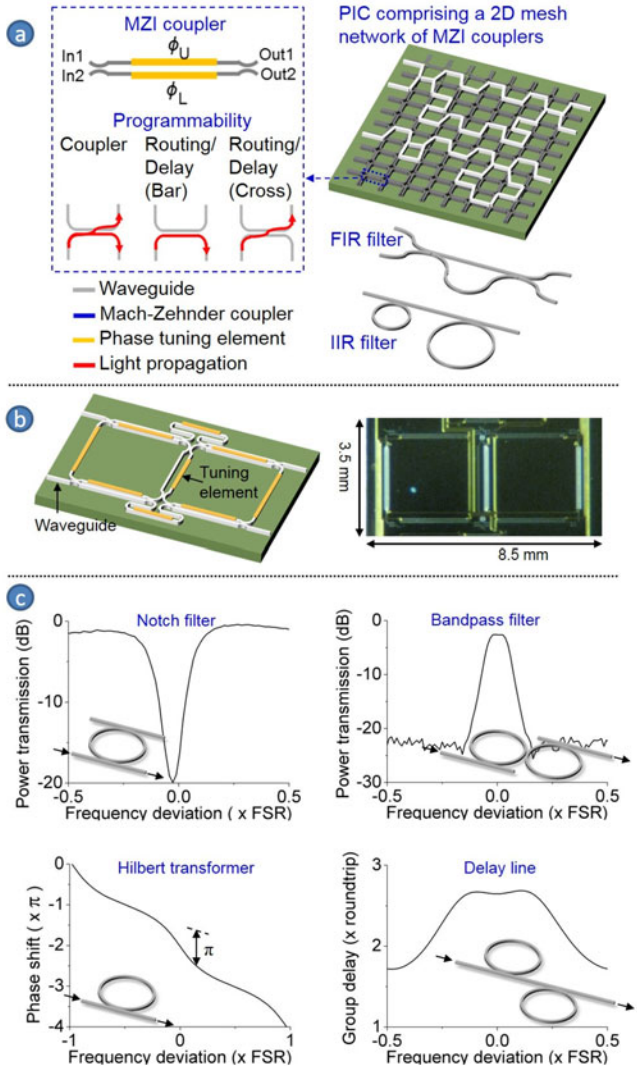

Fig. 16. (a) Concept of programmable optical chips. (b) a proof-of-concept device fabricated in TriPleX technology. (c) experimental verification of functional programmability.

To find practical applications in existing microwave systems, integrated MWP devices need to satisfy a number of stringent performance metrics including low insertion loss, high signal-to-noise ratio, and high linearity to maintain signal quality [44]. In RF photonics, these requirements translate to a high RF link gain, a low noise figure (NF), and a high spurious-free dynamic range (SFDR). Achieving on-chip functionalities with these stringent requirements has been proven challenging due to excessive insertion losses of functional photonic circuit. Recently, the first integrated MWP filter with fully-optimized RF performance, exhibiting an RF gain of 8 dB, a record-low NF of 15.6 dB, and a record-high SFDR of 116 dB.Hz$^{2/3}$, was reported [45]. This unparalleled performance is simultaneously obtained with advanced notch filtering functions featuring dual independently tunable stop-bands, each with a rejection of $>$50 dB and a high spectral resolution of 150 MHz. The key to these

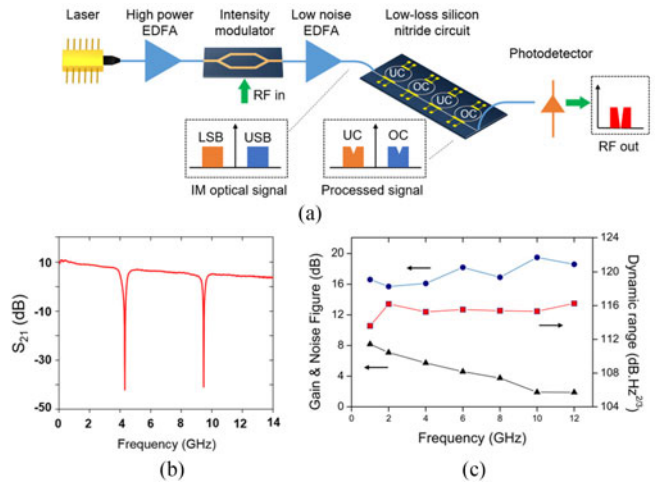

Fig. 17. (a) Schematic of experimental realization of the integrated RF photonic filter with spectra measured at different points. LSB: lower sideband; USB: upper sideband; UC: under-coupled; OC: over-coupled. Spectra of (b) dual-band filter with high extinction and resolution, and (c) measured RF gain, NF and SFDR over the entire tuning range.

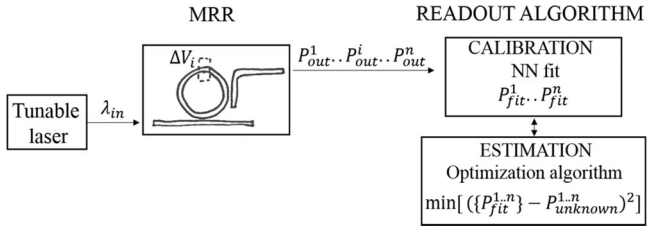

Fig. 18. Implementation scheme of a wavelength meter based on a single MRR and a Neural Network (NN) readout algorithm. For each input wavelength a set of transmitted powers, each corresponding to a heating voltage, is measured and used as calibration data that are fitted by the NN. In case of an unknown input wavelength the set of transmitted powers is given to an optimization algorithm that, in order to estimate the unknown wavelength by searching for the minimum in the error distribution.

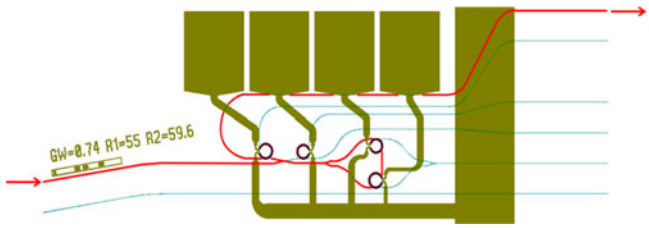

Fig. 19. Waveguide circuit used for an extended-range wavelength meter based on two MRRs in Vernier configuration. The red trace shows the light path, extending from the input on the left, passing through the Vernier filter, and leaving the circuit through a directional coupler towards the right-hand side. Shown in green are the electric contact pads which enable to apply two adjustable voltages (to thermally tune the resonant frequencies of the rings with two heating currents).

breakthrough results is the use of a low-loss silicon nitride TriPleX circuit consisting of series of ring resonators as optical filtering units with unique phase responses. The loss in the ring resonators plays a key role in determining the chip insertion loss and the quality factor of the ring. The waveguide geometry used in this work was the symmetric double-stripe waveguide (Section II-C) with loss of 0.1 dB/cm and ring bend radius of 125 microns. This leads to a ring filter with FSR of 25 GHz and quality factor of >900,000 allowing high resolution filtering of 150 MHz. Operating this circuit in conjunction with low-biasing of a Mach-Zehnder modulator (MZM) allows noise figure optimization technique to be achieved simultaneously with advanced filtering [44], [45]. The schematic of the integrated MWP filter is shown in Fig. 17(a).

The demonstrated dual-band filter with high rejection, achieved with 4 low-loss ring resonators, is shown in Fig. 17(b). Due to the low waveguide propagation loss, the filter width can be as low as 150 MHz. The measured RF gain, noise figure and dynamic range of the filter in the range of 1–12 GHz is shown in Fig. 17(c). The filter consistently achieved RF amplifications in the filter passband over the entire band of interest, with NF variations of 15.6–19.5 dB and SFDR variations of 113–116 dB.Hz$^{2/3}$.

G. Planar Waveguide Based Sensor

The monitoring of the wavelength of light is crucial for many applications such as in optical communications [46], wavelength-division-multiplexing [47], specifically for real-time wavelength control and tuning of on-chip hybrid lasers [48]. As shown in previous work [49], [50], a single micro-ring resonator (MRR) can be used as high-precision integrated wavelength meter [49] with reproducible and thermal-drift immune response [50]. In these cases the optical response (transmitted power vs wavelength) is evaluated with a readout algorithm that comprises a neural network (NN) as fit function of the calibration data, and an optimization algorithm, for determining the unknown input wavelength (Fig. 18).

An advantage of using MRR is the possibility to realize wavelength meters via high-Q resonators that can offer a smaller footprint and a much higher resolution as compared to other integrated optic approaches such as, e.g., Mach-Zehnder interferometers.

Previous results have led to a wavelength meter working within a relatively small wavelength range (∼1.5 nm) but with precision (50 pm) and ∼0.3 nm resolution. The named estimation range, however, would not be sufficient for many applications, e.g., monitoring on-chip hybrid lasers across the entire C-band that comprises tens of nanometers. We note that the estimation range of such wavelength meter is limited to a few nanometers, if based on a single MRR. This is limited by the largest FSR that can be realized with a single MRR as given by curvature loss.

In order to extend the estimation range of such wavelength meter it is thus required to extend the FSR with a different device structure, for which we used two coupled MRRs in a Vernier configuration as shown in Fig. 19.

In Fig. 20 shows an example of a measured transmission spectrum in comparison with a calculated spectrum. It can be clearly seen that the FSR has become much wider compared to previous work, reaching a value of 43 nm.

To investigate the described circuit with regard to its readout properties, a NN approach is used. The wavelength meter was first calibrated with 1001 different known input wavelengths, by

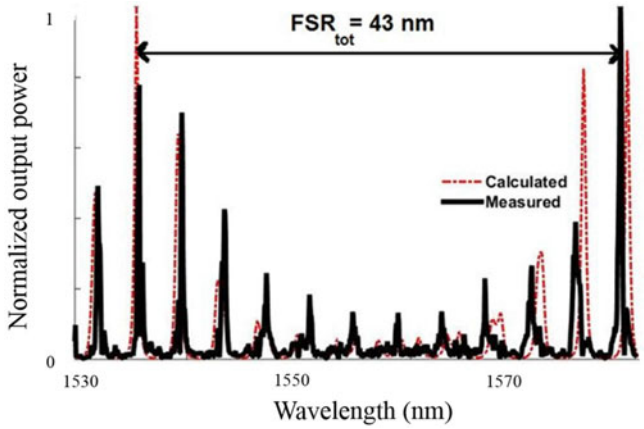

Fig. 20. Transmission spectra of the waveguide structure shown in Fig. 19. The black thick line is the experimentally acquired spectrum while the red dashed line shows the transmission as calculated from the manufacturing specifications. The small deviation of the two spectra is within the fabrication errors. An overall FSR of 43 nm is found, much greater than the FSR with a single MRR (2.6 nm).

recording the circuit transmission per single wavelength with 49 different combinations of the heating voltages for the two ring resonators. The wealth of the acquired data, i.e., transmitted power versus input wavelength at 49 heater settings, was then represented by the response of a NN. The expectation is that the range of correct readout of unknown wavelengths would be much wider than 1.5 nm, due the much increased FSR. Below we compare the performance of two types of readout algorithms. In the first, as in previous work, the search and optimization algorithm relies on minimizing the deviation between the calibrated (trained) NN response and the measured transmission for injected unknown wavelengths. The second uses the calibration measurement data directly, i.e., without a NN fit as look-up table, to minimize the deviation and thereby identify unknown wavelengths.

The graphs in Fig. 21 summarize the fidelity of the resulting wavelength estimation for the first and second case (top and bottom respectively). For comparison, the blue line indicates the response of an ideal wavelength meter. In the first case (NN) it can be seen that the estimation range is indeed extended, however, only to about 2 nm while the estimation is relatively precise (about 130 pm). In the second case (look-up table approach) the range is significantly extended, up to about 45 nm. However, the average precision is now noticeably lower (about 200 pm) due to more cases with a larger readout error. Current work aims on combining the two estimation approaches, in order to provide both a wide estimation range and a high precision with the shown Vernier circuit as example. The derived optimized readout strategy may then be extended and generalized, for readout with other waveguide circuits. Specific examples would be MRRs with much higher Q value, such as in depicted in Fig. 5. Other options are circuits with a higher number of resonators, and involving MZIs.

VI. Integrated Systems & Applications

A. InP-TriPleX & Packaging

Low fiber to TriPleX PIC interface losses (∼1 dB) for both telecom (ADS/SDS, HIC) and visible (Single stripe, LIC)

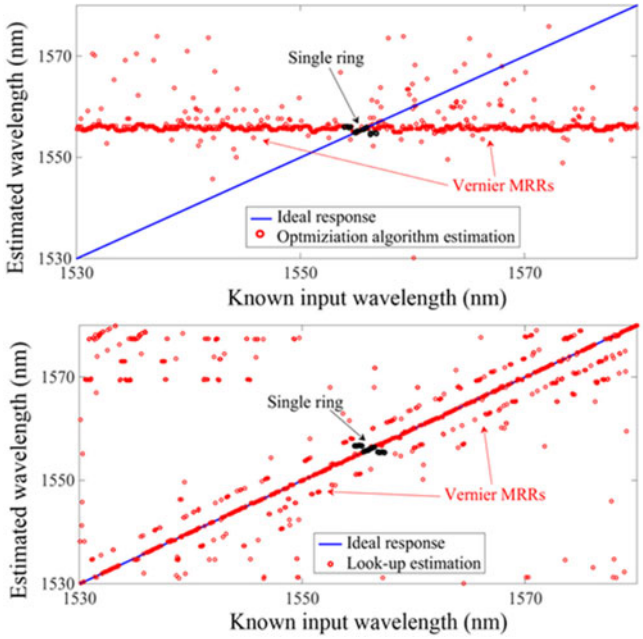

Fig. 21. Estimated wavelengths (red circles) versus known input wavelength for a NN fit and optimization algorithm (top) and for a look-up table method. The diagonal line corresponds to an ideal response where the estimated wavelength is exactly the same as that of the input. It can be clearly seen that the first case (top) provides a precise estimation but for a limited range, while the second case (bottom) provide a less precise estimation but for much wider range. Both cases however show an improvement in the estimation range compared to the case of a single ring (black circles).

applications can be achieved by tapering of the HIC TriPleX waveguides in both horizontal and vertical direction, as was pointed out in Sections II-B through II-D. The coupling losses between the TriPleX platform and different platforms such as InP, SOI, Polyboard, have been optimized to enable efficient hybrid integration. The hybrid integration allows for the combination of multiple material platforms and interfacing a broad range of waveguide technologies using TriPleX.

The advantage of hybrid integration is evident as shown in Fig. 22, showing a TriPleX optical beamforming network (1, Section C) having multiple hybrid interfaces to an array of InP detectors (2), a TriPleX spotsize converter (3), an InP modulator array (4) and a fiber array containing 23 single mode polarization maintaining fibers (5). Besides various optical interfaces, the DC and RF electrical interfacing is performed via gold wire bonds that are connected to separate printed circuit boards, whereas the thermal management takes place via a copper submount which is mounted onto a thermo-electric cooler (TEC).

Experimental data has been produced to confirm the numerical models we use to design the optimal taper structures. Fig. 23 shows the experimentally achieved interface loss between TriPleX and an InP high gain section, where the width of the waveguide at the chip facet in the TriPleX platform has been varied to match to the mode field of the InP gain section. An optimal configuration is found for a waveguide width of 2.7 μm providing a theoretical limit of ∼0.3 dB of hybrid interface loss. The discrepancy of 1.5 dB compared to the experimentally obtained loss of ∼1.8 dB is caused by the gap that was present between the InP and the TriPleX, which was in the order of 10 μm, caused by the submount on which the InP was flip chipped.

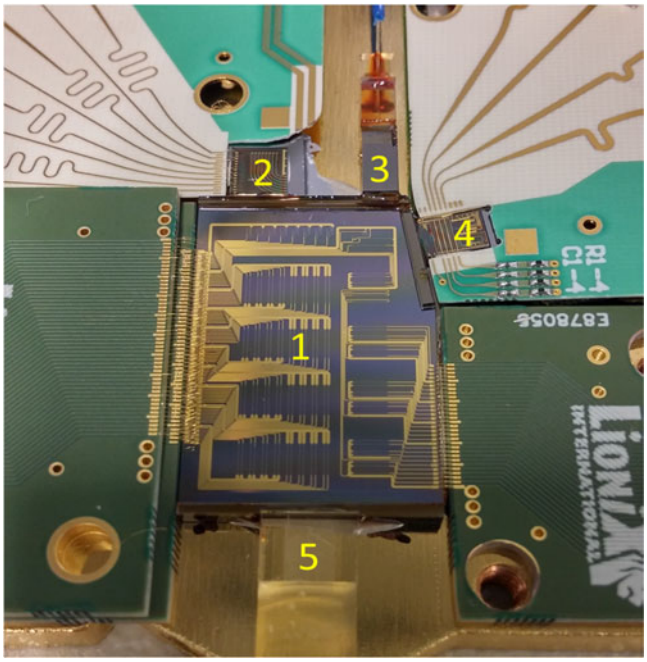

Fig. 22. Photograph of a TriPleX OBFN combining optical, electrical and thermal interfaces to various material platforms.

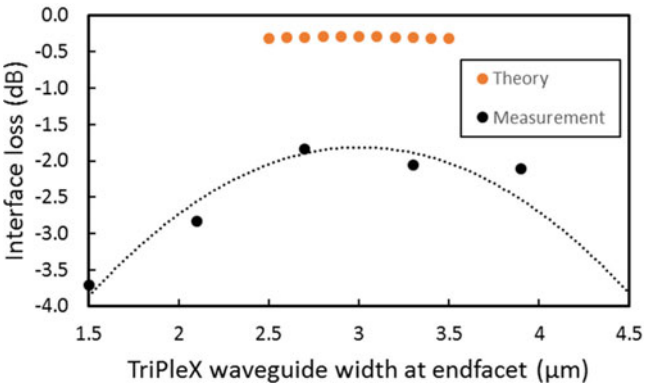

Fig. 23. Measured InP-TriPleX interface loss for various TriPleX waveguide widths.

Proper design of the InP submounts and mode matching of the TriPleX waveguides to the InP waveguide characteristics enable high coupling efficiency as can be seen in Fig. 23. The combination of the intrinsic low propagation loss of TriPleX waveguides and the high coupling efficiency to other technology platforms allows us to build very narrow bandwidth hybrid InP-TriPleX lasers, as will be further discussed in Section VI-B. Fig. 24 shows an example of a packaged and fiber pigtailed hybrid InP-TriPleX laser, having 2 optimized optical interfaces, i.e., the high gain InP (1) coupled to the TriPleX PIC (2) forming the hybrid tunable laser cavity and the TriPleX PIC coupled to the PM fiber output (3).

The working principle and specifications of the hybrid tunable laser will be described in the next section.

B. Tunable Hybrid Lasers With High Coherence

Enabled by the low-loss properties and the mature tapering options that offer high chip-to-chip coupling efficiency, TriPleX

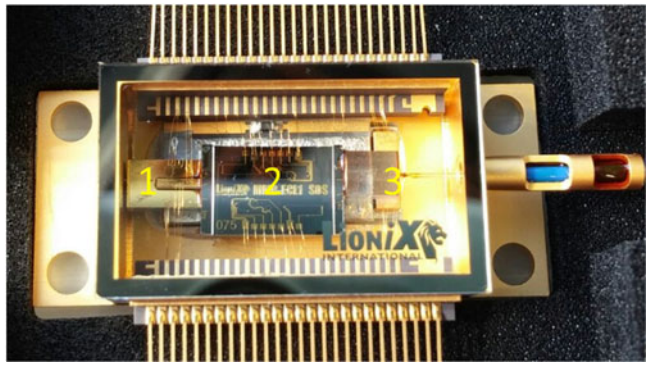

Fig. 24. Photograph of a fiber pigtailed hybrid tunable laser in a butterfly package containing a TEC and NTC for thermal control of the narrow linewidth laser cavity.

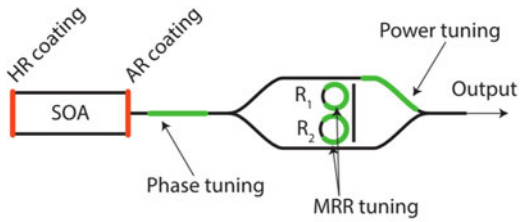

Fig. 25. Schematic diagram of a MRR-ECL. The thermal tuning elements in the external cavity are shown in green color ([53]).

is a highly suitable waveguide platform to realize external feedback circuits with long optical cavity lengths for bandwidth narrowing of diode lasers. When a semiconductor diode gain section is efficiently coupled to such a long TriPleX waveguide, the overall laser cavity shows an increased cavity lifetime. As a result, such hybrid lasers are able to provide laser light with a much higher spectral purity as compared to typical DFB and DBR lasers, i.e., single-mode oscillation with narrow spectral linewidth.

1) Laser Cavity Design: The typical waveguide circuit layout of such hybrid laser, is shown in Fig. 25 [48], [51], [52] and may be called Micro-Ring Resonator External Cavity Diode Laser (MRR-ECDL). In the experimental realization, the laser comprises an InP reflective semiconductor optical amplifier (RSOA) coupled to the external TriPleX waveguide circuit. The RSOA usually possess a HR coated back-facet to reduce cavity losses, and a low reflectivity front facet to impose lasing via the feedback from the external waveguide resonator circuit. A low reflectivity is achieved via an AR coating combined with a tilted facet.

The RSOA chip is butt-coupled to the TriPleX waveguide circuit, which carries a circuitry composed of two cascaded micro-ring resonators (MRRs) with slightly different radii, exploiting the Vernier effect as was also described above in Section G. Here the circuits are used as a highly frequency selective feedback mirror for imposing single-frequency operation at a narrow spectral linewidth. The two slightly different radii of the MRRS and their power coupling coefficients are selected such that a) the total free spectral range (FSR) of the Vernier mirror exceeds the 3 dB gain bandwidth of the RSOA, and b) that the

TABLE IV
OVERVIEW PERFORMANCE OF ASSEMBLED LASERS

Laser Assembly (year)	$\Delta\upsilon$ (kHz)	$\Delta\lambda$ (nm)	P(mW)	$SMSR$ (dB)
A (2013)	25	43	1	50
B (2014)	24	46	2	50
C (2016)	90	43	2	35
D (2016)	65	50	16	45

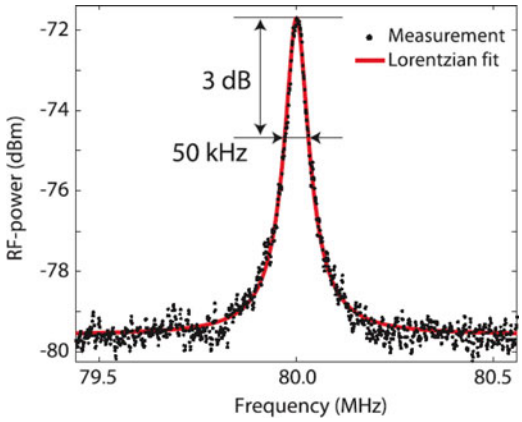

Fig. 26. Self-heterodyne beat spectrum of MRR-ECL assembly A. The black dots represent the measured RF-beat spectrum. A Lorentzian fit, red line, shows a 3-dB bandwidth of 50 kHz, corresponding to a laser bandwidth 25 kHz [51].

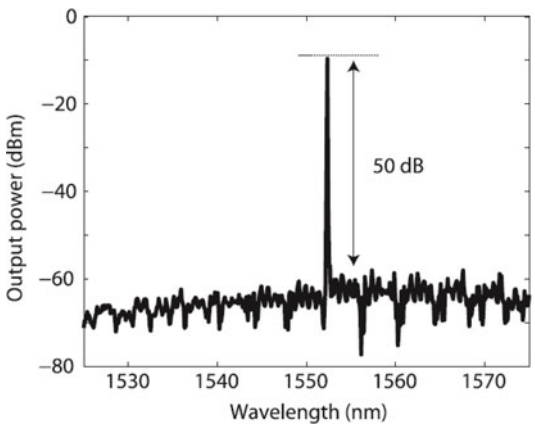

Fig. 27. Output power spectrum of the MRR-ECL assembly A. The measured side-mode suppression ratio is 50 dB [51].

reflectivity peaks next to the main Vernier peak are suppressed to avoid lasing at undesired side modes.

2) Laser Properties: In this section, we report on the experimental characterizations of chip-based InP-TriPleX hybrid lasers. Below we summarize the results of 4 similar laser assemblies (A to D) that differ with regard to their chip-to chip coupling efficiency, waveguide cross section and also type of SOA [48], [51], [52], [53]. A chronological overview of the results, including those of the other two assemblies, assembly B and C, are listed in Table IV.

A spectral linewidth of 25 kHz was obtained [51] with assembly A, see Fig. 26, with a side mode suppression ratio (SMSR) of 50 dB in Fig. 27. The output spectrum is shown in Fig. 28. An example of a large tuning range (50 nm) is reported with MRR-ECL assembly D and is shown in Fig. 28 [53].

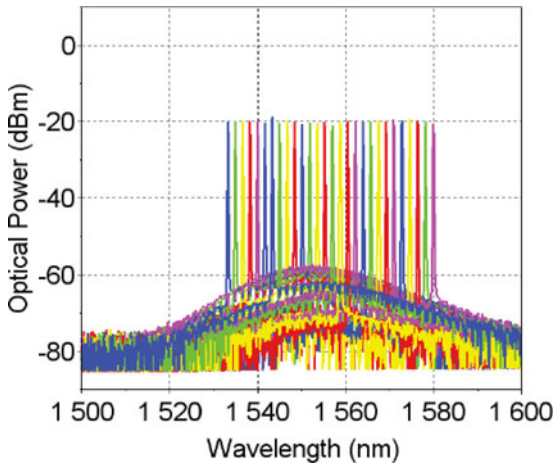

Fig. 28. Superimposed laser spectra of MRR-ECL assembly D. By thermal tuning, a wide wavelength range of around 50 nm is covered [53].

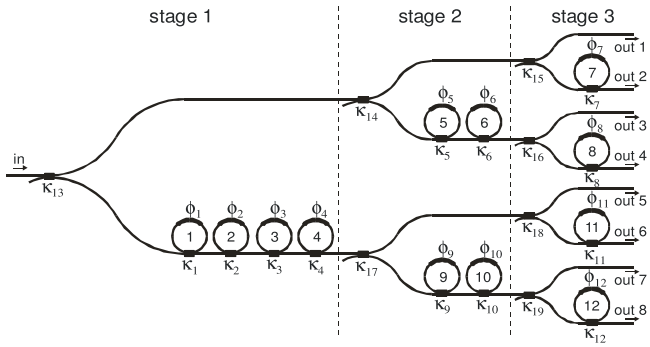

Fig. 29. Schematic diagram of a binary tree-based 1 × 8 OBFN for transmitter system. [24].

Because of the high Q value of the cascaded MRRs, the effective optical pathlength inside the cavity easily sums up to several cm. For this reason, low propagation loss waveguides (<0.2 dB/cm) are required. Another key to low cavity roundtrip losses is low-loss (<2 dB) chip-to-chip coupling as can easily be achieved with TriPleX through two-dimensional tapering.

The systematic reduction of losses, which is the key to proper intra-cavity filtering and long photon lifetimes, is what enables chip-based hybrid lasers with a very high degree of coherence involving spectral linewidths of well below 100 kHz. Current work explores laser feedback with TriPleX circuits of even lower loss and (<0.1 dB/cm) aims on further laser linewidth reduction [54].

C. Binary Tree Optical Beamforming Network

Phased array antenna systems can be found in multiple applications as radar systems, radio astronomy and communication systems like the upcoming 5G mobile networks systems. Optical beamforming networks (OBFN)s can be used to control the beam shape and direction. Fig. 29 shows a schematic diagram of a binary tree ring resonator based OBFN which has been manufactured in TriPleX [24].

This 1 × 8 binary tree OBFN divides the input signal over 8 outputs, where each output feeds an antenna port, thereby shaping and directing the beam. The use of cascaded ring

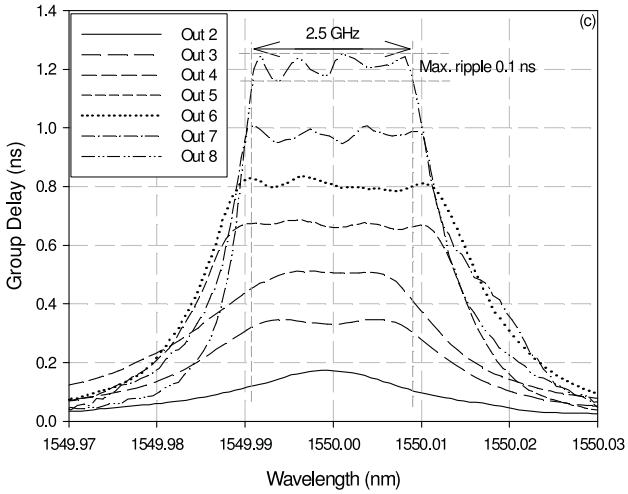

Fig. 30. Measured group delays at the output ports of the 1×8 OBFN. The rings are configured such that the delays cover a bandwidth of 2.5 GHz, with the largest delay value of approximately 1.2 ns and delay ripple of approximately 0.1 ns at the center wavelength of 1550.00 nm. [24].

resonators has two benefits [55]. First, for a certain target delay value the maximum delay bandwidth increases approximately linear with the number of ring resonators. Second, larger delays can be obtained by adding up multiple smaller delays which are generated by separate delay lines (ring resonators).

The manufactured OBFN has ring resonators with an FSR of 14 GHz. The ring resonators are fully programmable, both power coupling coefficient and roundtrip phase are tunable. By thermal-optic tuning linearly increasing delays from outputs 2 to 8 can be achieved where output 1 is the zero-delay reference, as shown in Fig. 30.

The ring resonators are tuned such that a linearly increasing delay is achieved over the 8 outputs, from 0 to 7 cascaded ring delays aligned to a wavelength of 1550.00 nm. The delays cover a bandwidth of 2.5 GHz, with the largest delay value of approximately 1.2 ns (corresponding to 36 cm distance in air) and delay ripple of approximately 0.1 ns (3 cm)). The TriPleX technology with waveguide losses well below 0.1 dB/cm makes even more complex OBFNs with larger delays feasible.

VII. OUTLOOK

The activities in the past decade have provided great insights in the possibilities and the capabilities of the TriPleX platform. Several appealing chip designs and photonic modules for different applications have been highlighted in this paper. The first goal is to disclose this platform technology to designers and photonic circuit architects and provide validated product design kits (PDKs) for the existing and new building blocks. The availability of new basic building blocks builds upon the release of a stable and reproducible front-end manufacturing process which is accessible through periodic multi-project wafer (MPW) runs.

The asymmetric double stripe (ADS) and local adiabatic tapering are enabling features that optimize the coupling to external components such as fibers and/or active materials. These PDKs will be released shortly to support hybrid platform and a higher confinement for tighter bending radii to increase the integration density, reduce the circuit footprint, and hereby reduce the cost of manufacturing.

Current research and development on the implementation of a stress-optic actuator for fast modulation has already proven to be at least 1000 times more power efficient than thermo-optic tuning, thus very attractive for complex processors such as Optical Beamforming Networks.

Assembly and Packaging are considered major challenges for development of a robust hybrid platform, especially when scaling to very complex hybrid processors where modulator-arrays, detector-arrays and gain sections monolithically integrated on InP.

Manufacturing of these relatively large chips requires investments in manufacturing, testing, inspection and automation in order to stabilize and mature the front-end processes and bring the yield to acceptable levels.

Moreover, modelling and measurements on RF-performance and thermal behavior of the assemblies and modules is key to develop robust solutions for automotive, life sciences and space applications.

In the end all challenges in integrated photonics are related to different fields of expertise, such as materials science and engineering. Challenges and solutions evolve out of combined expertise of multidisciplinary teams. The examples and work presented in this paper are the results of collaborations and intensive research in the past decade.

REFERENCES

[1] B. Bateman, "Silicon photonics, business situation report," *EAF LLC*, Feb. 2017. [Online]. Available: www.eaf-llc.com/silicon-photonics-market-situ/

[2] P. Muñoz *et al.*, "Silicon nitride photonic integration platforms for visible, near-infrared and mid-infrared applications," *Sensors*, vol. 17, no. 9, 2017, Art. no. 2088.

[3] S. Koehl, V. Krutul, and M. Paniccia, "Continuous silicon laser," *Intel White Paper*, 2005. [Online]. Available: www.intel.com/content/dam/www/public/us/en/documents/intel-research/Silicon-Laser_WhitePaper.pdf

[4] K. Wörhoff, R. G. Heideman, A. Leinse, and M. Hoekman, "TriPleX: A versatile dielectric photonic platform," *Adv. Opt. Technol.*, vol. 4, no. 2, pp. 189–207, 2015.

[5] F. Morichetti *et al.*, "Box-shaped dielectric waveguides: A new concept in integrated optics?," *J. Lightw. Technol.*, vol. 25, no. 9, pp. 2579–2589, Sep. 2007.

[6] D. A. I. Marpaung, C. G. H. Roeloffzen, A. Leinse, and M. Hoekman, "A photonic chip based frequency discriminator for a high performance microwave photonic link," *Opt. Express*, vol. 18, no. 26, pp. 27359–27370, 2010.

[7] R. G. Heideman *et al.*, "Low loss, high contrast optical waveguides based on CMOS compatible LPCVD processing: Technology and experimental results," in *Proc. IEEE/LEOS Benelux Ann. Symp.*, 2005, pp. 71–74.

[8] J. F. Bauters *et al.*, "Ultra-low-loss high-aspect-ratio Si_3N_4 waveguides," *Opt. Express*, vol. 19, no. 4, pp. 3163–3174, 2011.

[9] J. F. Bauters *et al.*, "Planar waveguides with less than 0.1 dB/m propagation loss fabricated with wafer bonding," *Opt. Express*, vol. 19, no. 24, pp. 24090–24101, 2011.

[10] J. F. Bauters *et al.*, "Ultra-low-loss single-mode Si_3N_4 waveguides with 0.7 dB/m propagation loss," in *Proc. 37th Eur. Conf. Expo. Opt. Commun.*, 2011, Paper Th.12.LeSaleve.3.

[11] 2018. [Online]. Available: http://www.lionix-international.com/mpw-service/

[12] [Online]. Available: http://www.phoenixbv.com/product.php?prodid=2300101&submenu=dk&prdgrpID=15&prodname=PDK%20-%20TriPleX%20

[13] 2018. [Online]. Available: http://www.phoenixbv.com/product.php?prodid=2300131&submenu=dk&prdgrpID=15&prodname=PDK%20LioniX%20International%20(Packaging)

[14] L. Zhuang *et al.*, "Low-loss, high-index-contrast Si_3N_4/SiO_2 optical waveguides for optical delay lines in microwave photonics signal processing," *Opt. Express*, vol. 19, no. 23, pp. 23162–23170, 2011.

[15] R. G. Heideman *et al.*, "Low loss, high contrast optical waveguides based on CMOS compatible LPCVD processing," in *Proc. Eur. Conf. Integr. Opt.*, 2007, Paper WB0-42.

[16] R. G. Heideman *et al.*, "Large-scale integrated optics using TriPleX waveguide technology: From UV to IR—Invited paper," *Proc. SPIE*, vol. 7221, Art. no. 72210R1.

[17] L. Zhuang *et al.*, "Novel ring resonator-based integrated photonic beamformer for broadband phased array receive antennas—Part II: Experimental prototype," *J. Lightw. Technol.*, vol. 28, no. 1, pp. 19–31, Jan. 2010.

[18] N. Hosseini *et al.*, "Stress-optic modulator in TriPleX platform using a piezoelectric lead zirconate titanate (PZT) thin film," *Opt. Express*, vol. 23, no. 11, pp. 14018–14026, 2015.

[19] S. R. Davis, G. Farca, S. D. Rommel, S. Johnson, and M. H. Anderson, "Liquid crystal waveguides: New devices enabled by >1000 waves of optical phase control," in *Proc. SPIE*, vol. 7618, pp. 76180E-1–76180E-14, 2010.

[20] T. H. Chao *et al.*, "Compact liquid crystal waveguide based Fourier transform spectrometer for in-situ and remote gas and chemical sensing," in *Proc. SPIE*, vol. 7508, pp. 75080K-1–75080K-11, 2009.

[21] J. P. Epping *et al.*, "Ultra-low-power stress-optics modulator for microwave photonics," in *Proc. SPIE*, vol. 10106, 2017, Art. no. 101060F.

[22] D. H. A. Blank, M. Dekkers, and G. Rijnders, "Pulsed laser deposition in Twente: From research tool towards industrial deposition," *J. Phys. D, Appl. Phys.*, vol. 47, no. 3, 2014, Art. no. 034006.

[23] M. Burla *et al.*, "On-chip CMOS compatible reconfigurable optical delay line with separate carrier tuning for microwave photonic signal processing," *Opt. Express*, vol. 19, no. 22, pp. 21475–21484, Oct. 2011.

[24] L. Zhuang *et al.* "Single-chip ring resonator-based 1x8 optical beam forming network in CMOS-compatible waveguide technology," *IEEE Photon. Technol. Lett.*, vol. 19, no. 15, pp. 1130–1132, Aug. 2007.

[25] L. Chrostowski *et al.*, "Silicon photonic resonator sensors and devices," in *Proc. SPIE*, vol. 8236, 2012, Art. no. 823620.

[26] E. Engin *et al.*, "Photon pair generation in a silicon micro-ring resonator with reverse bias enhancement," *Opt. Express*, vol. 21, no. 23, pp. 27826–27834, Nov. 2013.

[27] W. C. Jiang, X. Lu, J. Zhang, O. Painter, and Q. Lin, "Silicon-chip source of bright photon pairs," *Opt. Express*, vol. 23, no. 16, pp. 20884–20904, Aug. 2015.

[28] A. A. Savchenkov *et al.*, "Low threshold optical oscillation in a whispering gallery mode CaF_2 resonator," *Phys. Rev. Lett.*, vol. 93, 2004, Art. no. 243905.

[29] A. Boskovic, S. V. Chernikov, J. R. Taylor, L. Gruner-Nielsen, and O. A. Levring, "Direct continuous-wave measurement of n_2 in various types of telecommunication fiber at 1.55 μm," *Opt. Lett.*, vol. 21, pp. 1966–1968, 1996.

[30] M. A. G. Porcel *et al.*, "Two-octave spanning supercontinuum generation in stoichiometric silicon nitride waveguides pumped at telecom wavelengths," *Opt. Express*, vol. 25, pp. 1542–1554, 2017.

[31] J. P. Epping *et al.*, "On-chip visible-to-infrared supercontinuum generation with more than 495 THz spectral bandwidth," *Opt. Express*, vol. 23, no. 15, pp. 19596–19604, 2015.

[32] J. P. Epping *et al.*, "High confinement, high yield Si_3N_4 waveguides for nonlinear optical applications," *Opt. Express*, vol. 23, pp. 642–648, 2015.

[33] J. S. Levy *et al.*, "CMOS compatible multiple-wavelength oscillator for on-chip optical interconnects," *Nature Photon.*, vol. 4, pp. 37–40, 2010.

[34] L. Zhuang *et al.*, "Novel low-loss waveguide delay lines using Vernier ring resonators for on-chip multi-λ microwave photonic signal processors," *Laser Photon. Rev.*, vol. 7, no. 6, pp. 994–1002, 2013.

[35] G. Lenz, B. J. Eggleton, C. K. Madsen, and R. E. Slusher, "Optical delay lines based on optical filters," *IEEE J. Quantum Electron.*, vol. 37, no. 4, pp. 525–532, Apr. 2001, doi: 10.1109/3.914401.

[36] L. Zhuang, "Flexible RF filter using a nonuniform SCISSOR," *Opt. Lett.*, vol. 41, no. 6, pp. 1118–1121, 2016.

[37] L. Zhuang *et al.*, "Ring resonator-based on-chip modulation transformer for high-performance phase-modulated microwave photonic links," *Opt. Express*, vol. 21, no. 22, pp. 25999–26013, 2013.

[38] L. Zhuang *et al.*, "Sub-GHz-resolution C-band Nyquist-filtering interleaver on a high-index-contrast photonic integrated circuit," *Opt. Express*, vol. 24, no. 6, pp. 5715–5727, 2016.

[39] C. Taddei *et al.*, "Fully reconfigurable coupled ring resonator-based bandpass filter for microwave signal processing," in *Proc. 2014 9th Asia-Pacific Microw. Photon. Conf. Int. Topical Meeting*, 2014, pp. 20–23.

[40] Editorial, "A Birth of the programmable optical chip," *Nat. Photon.*, vol. 10, no. 1, 2016.

[41] L. Zhuang, C. G. H. Roeloffzen, M. Hoekman, K.-J. Boller, and A. J. Lowery, "Programmable photonic signal processor chip for radiofrequency applications," *Optica*, vol. 2, no. 10, pp. 854–859, 2015.

[42] J. Capmany and D. Novak, "Microwave photonics combines two worlds," *Nature Photon.*, vol. 1, pp. 319–330, 2007.

[43] D. Marpaung *et al.*, "Integrated microwave photonics," *Laser Photon. Rev.*, vol. 7, no. 4, pp. 506–538, 2013.

[44] Y. Liu, D. Marpaung, A. Choudhary, and B. J. Eggleton, "Lossless and high-resolution RF photonic notch filter," *Opt. Lett.*, vol. 41, no. 22, pp. 5306–5309, 2016.

[45] Y. Liu, J. Hotten, A. Choudhary, B. J. Eggleton, and D. Marpaung, "Lossless integrated RF photonic filter with record-low noise figure and 116 dB of dynamic range," presented at the CLEO-Pacific Rim, San Jose, CA, USA,2017.

[46] N. Ophir *et al.*, "Wavelength conversion and unicast of 10-Gb/s data spanning up to 700 nm using a silicon nanowaveguide," *Opt. Express*, vol. 20, no. 6, pp. 6488–6495, Mar. 2012.

[47] X. J. Gu, "Wavelength-division multiplexing isolation fiber filter and light source using cascaded long-period fiber gratings," *Opt. Lett.*, vol. 23, no. 7, pp. 509–510, Apr. 1998.

[48] Y. Fan *et al.*, "A hybrid semiconductor-glass waveguide laser," in *Proc. SPIE*, vol. 9135, 2014, Art. no. 91351B.

[49] R. M. Oldenbeuving *et al.*, "High precision wavelength estimation method for integrated optics," *Opt. Express*, vol. 21, no. 14, pp. 17042–17052, Jul. 2013.

[50] C. Taballione *et al.*, "Temperature-drift-immune wavelength meter based on an integrated micro-ring resonator," *Proc. SPIE*, vol. 10242, 2017, Art. no. 1024206.

[51] R. M. Oldenbeuving *et al.*, "25 kHz narrow spectral bandwidth of a wavelength tunable diode laser with a short waveguide-based external cavity," *Laser Phys. Lett.*, vol. 10, no. 1, 2013, Art. no. 015804.

[52] Y. Fan *et al.*, "Optically integrated InP-Si_3N_4 hybrid laser," *IEEE Photon. J.*, vol. 8, no. 6, 2016, Art. no. 1505111.

[53] J. L. Zhao *et al.*, "Narrow-linewidth widely tunable hybrid external cavity laser using Si_3N_4/SiO_2 microring resonators," in *Proc. IEEE 13th Int. Conf. Group IV Photon.*, Shanghai, China, 2016, pp. 24–25.

[54] Y. Fan *et al.*, "290 Hz intrinsic linewidth from an integrated optical chip-based widely tunable InP-Si_3N_4 hybrid laser," in *Proc. Conf. Lasers Electro-Opt.*, San Jose, CA, USA, 2017, Paper JTh5C.9.

[55] C. G. H. Roeloffzen *et al.*, "Silicon nitride microwave photonic circuits," *Opt. Express*, vol. 21, pp. 22937–22961, 2013.

Chris G. H. Roeloffzen received the M.Sc. degree in applied physics from the University of Twente , Enschede, The Netherlands, in 1998 and the Ph.D. degree in electrical engineering in 2002. He became an Assistant Professor with the Telecommunication Engineering Group, University of Twente, in 2002, where he was involved with research and education on integrated microwave photonic systems. He founded the company SATRAX, a spin-off of the University of Twente in 2009, where he was CTO. SATRAX, LioniX, and XiO Photonics merged into LioniX International in 2017. He is now a Chief Scientific Officer of LioniX International. He has authored or co-authored 40 refereed journal publications and more than 100 conference papers, and delivered 13 invited talks in various international conferences. He is the Technical Program Committee co-chair of IEEE Topical Meeting of Microwave Photonics. He is a MC member of the EU COST 16220: European Network for High Performance Integrated Microwave Photonics.

Marcel Hoekman studied applied physics at the University of Twente, Enschede, The Netherlands, and received the Graduate degree from the Integrated Optical Micro Systems Group, University of Twente, in 1998. From 2004 to 2009, he has been a part-time Ph.D. student with the Integrated Optical Micro Systems Group, University of Twente in the framework of the STW project "Multi-Sensing Arrays of Separately Accessible Optics Sensors." He finished a Post Graduate Design Program at the Integrated Optical Micro Systems Group that was based on the design of an integrated optical electro-optical modulator based on PZT containing multilayer-stacks, in 2001. In this project, he worked together with the group Experimental Solid State Physics III, Radboud University Nijmegen, The Netherlands. He joined Lion Photonix Technologies BV, in 2001, which was renamed to LioniX BV since 2002 and to LioniX International BV since 2016—as a Design Engineer. Besides simulation and mask design, he has experience in several cleanroom manufacturing processes and characterization methods, and he has worked as a Project Leader on several projects.

Edwin J. Klein received the M.Sc. degree from the Department of Electrical Engineering, University of Twente, Enschede, The Netherlands, in 2002 and received the Ph.D. degree from the Integrated Optical MicroSystems Group, University of Twente, in 2008. He was closely involved in the founding of LioniX International Photonics B.V., where he was working as the Vice-President of Research & Development since 2008. He has (co)authored more than 45 publications in journals and conferences and (co)holds five patents. His research interests include the development and practical application of complex photonic devices at visible and near-infrared wavelengths.

Lennart S. Wevers received the M.Sc. degree in applied physics from the University of Twente, Enschede, The Netherlands, in 2015. He joined LioniX BV in 2014, which was merged into LioniX International in 2017, as a Design Engineer specialized in optical designs.

Roelof Bernardus Timens received the M.Sc. degree in electrical engineering with specialization microwave photonics and the Ph.D. degree in electromagnetic compatibility both from the University of Twente, Enschede, The Netherlands, in 2009 and 2013, respectively. He continued his academic career with a 1 year Postdoctoral in electromagnetic compatibility. Since September 2014, he has been with SATRAX, nowadays LioniX International, as a Design Engineer in the fields of microwave photonics and photonic integration. His competences vary from functional design and modeling of integrated optical systems including RF interfaces to the specification, verification, and demonstration of products in the laboratory. Furthermore, he is internal Project Leader on several national and European projects.

Denys Marchenko received the M.Sc. degree in applied physics and mathematics from the Moscow Institute of Physics and Technology, Dolgoprudny, Russia, in 2010, and the Ph.D. degree in the field of applied physics from Radboud University Nijmegen, Nijmegen, The Netherlands, in 2014. His thesis is entitled "Laser-based methods for sensitive trace gas detection." He joined LioniX International as a Design Engineer/Project Manager in 2014, and currently he is involved in a few European projects with the main focus on biochemical sensing and telecom applications. Besides, his expertise includes a wide range of cleanroom manufacturing processes and tools.

Dimitri Geskus received the B.Eng. degree in applied physics from Saxion Hogescholen, Enschede, The Netherlands, in 2003, the M.Sc. degree in applied physics and the Ph.D. degree from the University of Twente, Enschede, in 2006 and 2011, respectively. From 2010 to 2012, he was a Product Engineer at Xiophotonics, Enschede, The Netherlands, followed by having a Postdoctoral position at Centro de Lasers e Aplicações—Instituto de Pesquisas Energéticas e Nucleares, São Paulo, Brazil, until 2014. From 2014 to 2016, he was a Researcher with KTH Royal Institute of Technology, Stockholm, Sweden. He is currently a Design Engineer/Project Manager at LioniX International, Enschede, The Netherlands. His expertise is in field of laser physics, photonic integrated systems, packaging, and interfacing of PICs. He was awarded the personal grant for young talents from the scientists without borders program of CNPq, Brazil, in 2012.

Ronald Dekker received the B.Sc. degree in applied physics and the Ph.D. degree in integrated optics from the University of Twente, Enschede, The Netherlands.

He worked several years at the MESA+ Research Institute for Nanotechnology, University of Twente as a Process Engineer on the development of novel clean room processing steps for the IC-industry to improve the quality of flat panel displays. Hereafter, he was employed at JDS Uniphase, both in the Netherlands and Canada where he worked on the development of MEMS-based variable optical attenuators and a new fabrication platform for low-cost dense wavelength division multiplexers (DWDM) systems. Later, as a Quality Engineer, he was also responsible for all reliability and quality issues related to the DWDM systems at JDS Uniphase. He became a Senior Researcher at the Research Chair Integrated Optical Micro Systems (University of Twente) working on femtosecond waveguide writing in rare-earth doped optical materials. After that, he joined LioniX BV where he led multidisciplinary projects in the field of integrated optics and microfluidics for both telecommunication and biomedical applications. He has been active in the field of material engineering, microfabrication, integrated optics, packaging, and assembly for more than 20 years. In 2010, he was a CTO of XiO Photonics, where he has been working extensively on standardization and assembly methods for integrated optics. After the merge of LioniX BV, XiO Photonics BV, and SatraX BV into LioniX International BV he is responsible for the assembly of integrated optical modules for visible light applications, telecom applications, and hybrid integration.

Andrea Alippi received the Graduate degree in telecommunications engineering from Politecnico di Milano, Milano, Italy, in 2015, with a thesis on the development of a testing technique for the qualification of manufacturing processes for photonic circuits at wafer level. He joined the Photonic Devices Group in the same year. Following the path of packaging of Photonic Integrated Circuits (PICs), he is now a Process Packaging Engineer and a Project Manager at LioniX-International. He has a broad experience in testing and characterization of PICs both in the electrical and optical domain. He did develop skills in assembly and production chain regarding PIC packaging achieved operating on fiber-to-chip alignment stages, wire-bonding, and polishing machines. His main research interests include the analysis of mechanical stresses induced by thermal gradients inside packages, the study of an integrated MUX/DEMUX transceiver based on indium phosphide technology exploiting few-mode transmission fiber, and in general the modeling, design, and characterization of PICs for many applications from telecom and visible light to space and healthcare.

Robert Grootjans was born in Oldenzaal, The Netherlands, in 1989. He received the B.Sc. and M.Sc. degrees in electrical engineering from the University of Twente, Enschede, The Netherlands, in 2016. Since 2016, he has been working as a Design Engineer for microwave photonic systems in LioniX International, Enschede.

Albert van Rees was born in Zwolle, The Netherlands, in 1984. He received the B.Sc. degree in applied physics from the University of Twente, Enschede, The Netherlands, in 2010. He is currently working toward the M.Sc. degree by following the optics and biophysics master's programme with the same university. He joined XiO Photonics in 2009, which was merged into LioniX International in 2017 as a Design Engineer. He has experience in simulation, design, and characterization of photonic integrated circuits.

Ruud M. Oldenbeuving received the B.Sc., M.Sc., and Ph.D. degrees from the Laser Physics and Nonlinear Optics Group, University of Twente, Enschede, The Netherlands, in 2005, 2008, and 2018, respectively. His work focused on external cavity diode lasers. After graduation for his Ph.D., he used his expertise to develop optical beam forming networks in TriPleX and hybrid TriPleX-InP laser devices for several companies: SATRAX B.V. (2013–2017), LioniX B.V. (2016–2017), and LioniX International (currently).

Jörn P. Epping received the Diploma degree in physics from the University of Münster, Münster, Germany, in 2011 and the Ph.D. degree from University of Twente, Enschede, The Netherlands, in 2015 with focus on nonlinear optics in integrated waveguides. Since 2015, he has been working as a Design Engineer for LioniX BV and LioniX International.

René G. Heideman received the M.Sc. and Ph.D. degrees in applied physics from the University of Twente, Enschede, The Netherlands, in August 1988 and January 1993, respectively. He is an expert in the field of MST, based on more than 25 years of experience. He specializes in Integrated Optics, covering both (bio-) chemical sensing and telecom applications. He is the Inventor of the TriPleX Technology, coauthor of more than 250 papers, and holds more than 25 patents in the IO-field, in more than ten different subjects. From 2001 to 2016, he was a CTO of LioniX BV, which he co-founded in 2001. Since 2016, he has been a CTO of LioniX International BV. Since 2008, he has been the board member (CTO) of Panthera BV, a group a high-tech innovative companies focusing on creating new business based on micro/nanotechnology. Since June 2012, he has been a Visiting Professor Nanotechnology, Saxion University of Applied Sciences, Enschede, The Netherlands. He is a member of several Dutch and European steering committees and, among others, board member of MinacNed (Dutch association for microsystems and nanotechnology) and BOS-member of the European Consortium Photonics21.

Kerstin Wörhoff received the M.Sc. degree in electrical engineering and the Ph.D. degree in applied physics in 1991 and 1996, respectively. Between 1996 and 2000, she worked as a Postdoctoral Researcher with the Lightwave Devices Group, University of Twente, Enschede, The Netherlands, with research focus on photonics technology development for telecom applications. In 2000, she became an Assistant Professor in Integrated Optics, University of Twente and was involved in various European as well as national research projects. Her research interests include development and optimization of photonics technologies for a wide range of active and passive integrated optical functionalities, optical waveguide design as well as project management and teaching in materials science and technology. In 2013, she joined LioniX BV as a Project Manager and a Design Engineer.

Arne Leinse was born in the Netherlands in 1977. He received the Master of Physics degree from the University Twente, Enschede, The Netherlands, and the Ph.D. degree from that same university in the Integrated Optical Microsystems Group in 2001 and 2005, respectively. His Ph.D. thesis was titled: "Polymeric microring resonator based electro-optic modulator." His Ph.D. thesis was titled: "Polymeric microring resonator based electro-optic modulator." Hereafter, he joined LioniX BV where he was involved in the invention and development of the TriPleX platform from the beginning. He has been involved from the original concept until the exploitation and (co)authored more than 100 articles in the last years. He is active in integrated optics for more than 15 years. He has been the Vice-President of LioniX BV in the last years and since the establishment of LioniX-International in Enschede, the Netherlands, in 2016 and currently a Chief Commercial Officer.

Douwe Geuzebroek received the Ph.D. degree in electrical engineering from the University of Twente, Enschede, The Netherlands, at the Integrated Optical MicroSystem Group on a topic of applying integrated optical microring resonators in telecommunication networks. He has more than 15 years of experience in integrated photonics and its applications, ranching from R&D to product development stages. He has a strong interest in matching the technical aspect of a technology to the needs of the market. In 2005, he joined LioniX BV as a Design Engineer and a Project Leader focusing on microring resonators and other integrated optical telecommunication devices and was actively involved in the start-up of XiO Photonics in 2008. As VP Marketing and Sales at XiO Photonics, he supported the development of the waveguide technology for visible light applications and the introduction of this technology in several products. He participated in several research projects both national and European.

He is currently working as VP Marketing & Sales at LioniX International where he is involved in the acquisition of new commercial and research projects for photonic integrated modules in life science, metrology, and telecommunication applications.

Erik Schreuder was born in Rijssen, the Netherlands in 1975 and studied applied physics at the University of Twente, Enschede, The Netherlands, where he received the M.Sc. degree from the Biophysical Engineering Group in 2003. In this same group, he started his Ph.D. work on the topic of advanced detection systems for the analysis of circulating tumors cells. His Ph.D. work was carried out in collaboration with Immunicon Corporation (Huntingdon Valley, PA, USA) and his thesis was titled: "Laser Image Cytometer for Analysis of Circulating Tumor Cell." In 2008, he joined LioniX B.V. which is changed in 2017 into Lionix International where he is currently working as a Group Leader in the field of micro fluidics, integrated optics, and optofluidics. He has experience in several cleanroom manufacturing processes and characterization methods, and he has worked as a Internal Project Leader on several national and European Project.

Paulus W. L. van Dijk was born in Tilburg, The Netherlands, in 1968. He received the B.S. and M.S degrees in applied physics from the Technical University Eindhoven, Eindhoven, The Netherlands, in 1992 and the Ph.D. degree in nuclear physics techniques in 1997 in the field of materials science and materials characterization using high energy ion beam analysis techniques. He received the Master of Business Marketing from TIAS Nimbas School, Eindhoven, in 2002. From 1997 to 1998, he was a R&D Engineer at High Voltage Engineering, Amersfoort, The Netherlands. He installed, calibrated, tested, and improved the first prototype Accelerometer Mass Spectrometers for Carbon Dating and Iodine Dating at the Japanese Atomic Energy Research Institute, Mutsu, Japan. From 1999 to 2010, he worked as a Product Marketing Manager at ASML where he was responsible for new business development and product marketing at the Special Applications and 300 mm Business Units. He started as a Chief Executive Officer and cofounder of SATRAX in 2010 with focus on development and marketing of integrated microwave photonics products. Since 2017, he has been a Vice President Strategy and Innovation at LioniX International in Enschede, The Netherlands. He coauthored more than 34 articles and holds 6 patents.

Ilka Visscher received the B.Eng. degree in electrical and electronic engineering with specialization applied communication engineering from the Saxion University of Applied Sciences, Enschede, The Netherlands, in 2012 and the M.Sc. degree in electrical engineering with specialization in telecommunication from the University of Twente, Enschede, Netherlands, in 2014. As a System Engineer at SATRAX B.V., she developed system specifications, design and implementation of integrated optical beam formers. She created the mask design of optical chips for different photonic integration platforms and was involved in the programming of the control electronics for the developed products. She was a Project Leader of several projects and since 2016 she has been working as Design Engineer and a Project Manager for LioniX International. Her research interests include managing projects and developing functional designs of integrated optics to the specification, verification and demonstration of products in the laboratory.

Caterina Taddei (M'12) was born in Castiglione del Lago, Italy, in 1984. She received the B.Sc. and M.Sc. degrees in information engineering and telecommunication & electronics engineering both from the University of Perugia, Perugia, Italy, in 2008 and 2012, respectively. She is currently working toward the Ph.D. degree in laser physics at Non-linear Optics Group, University of Twente, Enschede, The Netherlands. In 2012, she was an IT Consultant for British Telecom, Rome. Her Ph.D. research interests include microwave photonics and specifically it is about hybrid integrated optical beam-forming networks for phased array antennas systems, for satellite communications applications. From 2017, she collaborates with LioniX International on the development and testing of novel hybrid integrated systems for satellite communications systems.

Youwen Fan was born in Gong'an, Hubei, China, in 1988. He received the B.Eng. degree in optoelectronics information engineering in 2010 and the M.Sc. degree in optical engineering in 2013, from Huazhong University of Science and Technology, Wuhan, China, and the Ph.D. degree in applied physics from University of Twente, Enschede, The Netherlands, in 2017. Since 2017, he has been working as a Postdoctoral Researcher at the Laser Physics and Nonlinear Optics Group, University of Twente, and he also works as a Guest Researcher at LioniX International. His research interests include narrow-linewidth, chip-based hybrid lasers, semiconductor lasers subject to optical feedback or optical injection, modelling of complex semiconductor lasers, and coherent fiber-optic communications. He is a member of the Optical Society.

Caterina Taballione was born in Rome, Italy, in 1988. She received the B.S. and M.S. degrees in physics of matters from the University of Rome "La Sapienza," Rome, Italy, in 2014 with a thesis on quantum optics, studying the propagation of the orbital angular momentum of light through the atmosphere, and showing the resilience of hybrid qubits through atmospheric turbulence. Since 2015, she has been working toward the Ph.D. degree at the University of Twente, Enschede, The Netherlands, within the Laser Physics and Non Linear Optics group lead by Prof. K.-J. Boller.

Her research interests include advantages and properties of integrated microring resonators, Mach-Zehnder interferometers and arrayed waveguides, in order to build an on-chip spectrometer where the data readout is performed via a smart readout based on neural network and nonlinear optimization algorithm.

Yang Liu received the Bachelor's degree in optoelectronics from the Huazhong University of Science and Technology, Wuhan, China, in 2012, and the Master's degree in optical engineering from Wuhan National Laboratory for Optoelectronics, Wuhan, China, in 2015. He is currently working toward the Ph.D. degree in physics (through the USydIS Scholarship) in the Nonlinear Photonics Group, Centre for Ultrahigh Bandwidth Devices for Optical Systems, School of Physics, University of Sydney, Sydney, NSW, Australia. His research interests include the nonlinear and nonlinear optics in integrated photonics, and applications to microwave photonics. He is a member of the Executive Committee of the University of Sydney OSA and SPIE Student Chapter.

David Marpaung received the Ph.D. degree in electrical engineering from the University of Twente, Enschede, The Netherlands, in 2009. From 2009 to 2012, he was a Postdoctoral Researcher in the University of Twente within the framework of the European Commission FP7 funded project SANDRA, working on microwave photonic system integration for optical beamforming. He joined CUDOS University of Sydney, Australia, in August 2012 as a Research Fellow. He is currently a Senior Research Fellow leading the nonlinear integrated microwave photonics research activities in CUDOS University of Sydney. He has authored or coauthored 49 refereed journal publications and more than 80 conference papers, and delivered 25 invited talks in various international conferences. He is the technical program committee co-chair of IEEE Topical Meeting of Microwave Photonics (MWP 2018). He is the recipient of the 2015 Discovery Early Career Research Award from the Australian Research Council and the 2017 Vidi Award from the Netherlands Organisation for Scientific Research. His research interests include RF photonics, photonic integration, nonlinear optics, and phononics.

Leimeng Zhuang is currently a Senior Research Fellow with Electro-Photonics Laboratory, Monash University, Melbourne, VIC, Australia, working on the topic of hybrid integration platform combining electronics and photonics for high-speed, energy-efficient optical communication, and microwave photonic systems. From 2009 to 2014, he worked as a Research Fellow and a Product Specialist at the University of Twente, Enschede, The Netherlands, XiO Photonics B.V., SATRAX B.V. (currently LioniX International), and Netherlands Aerospace Laboratory, responsible for the development of a Ku-band satellite tracking phased array antenna system and integrated optical signal processors.

Meryem Benelajla was born in 1994 in Morocco. She received the M.Sc. (Hons.) degree from the University of Rennes, Rennes, France, and the M.Eng. (Hons.) degree from ENSSAT Engineering School, Lannion, France, both in photonics and nanotechnologies. She performed the M.Sc. and M.Eng. projects at Laser Physics and Nonlinear Optics, University of Twente, Enschede, The Netherlands, with work on integrated optical wavelength meters based on ring resonator circuits. Since November 2017, she has been with the Attocube Systems, Munich, Germany, as Early-Stage Researcher and Ph.D. student within the EU Innovative Training Network "4 Photon," where she develops confocal microscope systems that allow to control and analyze the polarization of semiconductor nanostructures.

Klaus-J. Boller received the M.Sc. degree in physics with experimental work on surface science, electron spectroscopy, and synchrotron radiation at Deutsches Elektronen-Synchrotron, Hamburg, Germany. He received the Ph.D. degree from the University of Hamburg, Hamburg, in 1988 with contributions on multimode laser intracavity spectroscopy, nonlinear optical conversion in alkali vapor, and with work on two-photon lasers. He spent two years at Stanford University as Postdoctoral Researcher where he demonstrated a major breakthrough in nonlinear optics, known as electromagnetically induced transparency. As a Research Group Leader in the University of Kaiserslautern, Kaiserslautern, Germany, starting from 1991, he focused on modern solid-state laser systems, high-power diode laser systems, quantum noise in diode lasers and on efficient conversion into various spectral ranges, particularly the IR and mid-IR with diode pumped optical parametric oscillators (OPOs). Specifically, he pioneered in demonstrating the first diode pumped OPOs and also the first fiber pumped continuous-wave OPOs. He was appointed as a Full Professor in 2000 and the Chair of the Laser Physics and Nonlinear Optics, University of Twente, Enschede, The Netherlands. Much of current work focuses on spectral and temporal control in integrated optical waveguide circuits. The latter comprises hybrid-integrated glass-diode lasers, microwave photonic circuits, all-optical switching and nonlinear optical conversion in waveguides. Recent achievements are the spectrally broadest supercontinuum ever generated on a chip, as well as hybrid diode lasers with narrow spectral linewidth.